Quaternary Science Reviews 293 (2022) 107725

Contents lists available at ScienceDirect

Quaternary Science Reviews

journal homepage: www.elsevier.com/locate/quascirev

# Mid to late Holocene climate variability, forest fires and floods entwined with human occupation in the upper Ganga catchment, India

Shubhra Sharma [a, *], S.P. Sati [b], N. Basavaiah [c], Shilpa Pandey [d], Y.P. Sundriyal [e], Naresh Rana [f], Priyanka Singh [d], Subhendu Pradhan [a], A.D. Shukla [g], R. Bhushan [g], Rakesh Bhatt [h], Navin Juyal [i]

[a] *Department of Geography, Institute of Science, Banaras Hindu University, Varanasi, 221005, India*
[b] *Department of Basic Science, College of Forestry Ranichauri, Tehri Garhwal, 249001, India*
[c] *Indian Institute of Geomagnetism, New Panvel, Navi Mumbai, 410218, India*
[d] *Birbal Sahni Institute of Palaeosciences, Lucknow, 226007, India*
[e] *Department of Geology, HNB Gharwal, Srinagar Gharwal, 246174, India*
[f] *Department of Geology, University of Delhi, Delhi, 110007, India*
[g] *Physical Research Laboratory, Ahmedabad, 380009, India*
[h] *Department of History, Culture and Archaeology, HNB Garhwal, Srinagar Gharwal, 246174, India*
[i] *Kabir Enclave, Bopal, Ahmedabad, 380058, India*

A R T I C L E I N F O

*Article history:*
Received 25 March 2022
Received in revised form
20 August 2022
Accepted 20 August 2022
Available online 5 September 2022

Handling Editor: Dr P. Rioual

*Keywords:*
Indian Summer Monsoon
Mid-Holocene
South-eastern Asia
Himalaya
Geomorphology
Neoglacial
Floods
Fires

A B S T R A C T

The present study attempts to understand the geomorphic response in the upper Ganga catchment to the mid-late Holocene (neoglacial) climate variability. The study infers five major phases of millennial-scale climate variability with centennial-scale inversions using geochemical and magnetic proxies from relict Lesser Himalayan Lake sediments. Phase-1 (6–4 ka) is marked by enhanced precipitation/runoff (increased allochthonous contribution) under a stronger Indian Summer Monsoon (ISM). The prominent reversal in the trend between ~5 and 4 ka includes global arid events such as 4.2 ka. Phase-2 (4–2.2 ka) shows a declining precipitation/runoff (decreased allochthonous input) under declining ISM with a prominent dip after ~3 ka. After phase-2 the climate reversals are distinct and of shorter (centennial) duration. For example, in Phase-3 (2.2–1.4 ka) improved ISM is inferred; Phase-4 (1.4–1.0 ka) is marked by a sharp decline in the ISM, and Phase-5 (<1.0 ka) includes centennial-scale events of Medieval Climate Anomaly (MCA) and the onset of Little Ice Age (LIA). The relative increase (decrease) in the concentration of geochemical and magnetic proxies is indicative of strengthened (weakened) ISM where relatively drier phases are in sync with the North Atlantic climate perturbations. We observed clustering of optically dated flood events around 6.5, 4.5, 2.6, 1.4, 0.8, and 0.4 ka which corresponds to periods of moderate ISM thus, suggesting a coupling between warm-humid monsoon and relatively dry westerlies. The relatively higher concentration of micro-charcoal in the lake sediments indicates widespread forest fires around 5.9–5.3, 4.5–4.3, 3.4–3.0, 2.0–1.5 and ~1 ka. Given the archaeological evidence of sedentary settlements since ~3 ka in the upper Ganga catchment, the study speculatively argues anthropogenic forcing for forest fires after 3 ka. Further, the highest probability flood phases succeed the fire events and may be indicative of enhanced vulnerability of the catchment to floods due to vegetation loss (enhanced erosion and surface runoff).



## 1. Introduction

The Indian Summer Monsoon (ISM) is a major component of the tropical climate system, including the Central Himalayas that significantly impacts the earth surface processes (e.g., Juyal et al.,

* Corresponding author.
*E-mail addresses:* shubshubhra@gmail.com, shubhra@bhu.ac.in (S. Sharma).

https://doi.org/10.1016/j.quascirev.2022.107725
0277-3791/

2010; Ray and Srivastava, 2010; Sundriyal et al., 2015). The response of the ISM is known to be modulated by cooling in the northern latitude, as it advances the cold front in the Indian subcontinent weakening the ISM, and vice-versa (Clemens and Prell, 2007; Zhisheng et al., 2011). The paleoclimatic archives from the Central Himalaya (Srivastava et al., 2017; Bhushan et al., 2018; Ghosh et al., 2020) indicate that the Himalayan ecosystem and associated geomorphic processes responded sensitively to the millennial and centennial synoptic-scale climate perturbations during the Holocene (Bond et al., 1997, 2001; Hong et al., 2003; Gupta et al., 2005).

The mid-Holocene period is particularly important to understand anthropogenic forcings, when a transition from hunter-gatherer to sedentary (cultivation-based) societies marked the onset of long-lasting anthropogenic environmental impact, mainly due to widespread forest clearing (Lewis and Maslin, 2015). For example, in the south-east Asian region after ~6 ka (Stephens et al., 2019) the early Indus valley civilization phase (~5.7–4.8 ka BP) (Kenoyer, 1998; Wright et al., 2008) is represented by pastoral and village farming communities (Meadow et al., 1991; Wright, 2010). In the mountains, where the terrain conducive for agriculture may be limited, often it is combined with pastoral activity leading to a substantial impact on the terrain (Knörzer, 2000). Further, the advent of multi-seasonal cropping in the mountains significantly impacted the ecosystem. For example, in the higher Himalayas (Jhong river valley), Nepal; > 3000 m above mean sea level (amsl) pollen evidence of two harvests per year requiring large-scale forest clearance was documented (Knörzer, 2000).

For the anthropogenic land cover change, often fire was used as a major tool in forest clearance (Bowman et al., 2011), which itself (as natural fires) has been an integral part of the ecosystems and biogeochemical cycles (Randerson et al., 2006; Scott and Glasspool, 2006; Jaffé et al., 2013). Fires and climate are suggested to have a direct relationship (Swetnam, 1993), while the role of vegetation is complex (Higuera et al., 2009). Besides, even subsistence gatherers are known to influence natural fire regimes under not-so-favourable climatic/landcover conditions (Dietze et al., 2018).

Studies from the upper Ganga catchment suggest that glaciers expanded marginally during the mid-Holocene (Sati et al., 2014; Bisht et al., 2015); the ISM was moderate with low amplitude fluctuations (Kathayat et al., 2017; Srivastava et al., 2017; Bhushan et al., 2018); and vegetation was dominated by non-woody plants (Ghosh et al., 2020). Therefore, it can be hypothesized that geomorphic response of the terrain particularly for extreme events such as floods and forest fires may be the result of a complex interplay of multiple factors. Further, the archaeological evidence indicates that the valley was occupied by sedentary human populations (Bhatt and Nautiyal, 1987; Nautiyal and Khanduri, 1986) involved in agricultural and pastoralism (Demske et al., 2016) and the terrain began to witness anthropogenically modulated land use/land cover changes. Thus, contributing positive feedback to the climate system by increasing methane/carbon dioxide flux from forest clearance and agricultural practices (Ruddiman and Thomson, 2001; Ruddiman, 2003; Kaplan et al., 2011; Ruddiman et al., 2011; Stephens et al., 2019). Another major consequence of forest (tall grasses and trees) clearing is an increased volume of streamflow leading to enhanced erosion (Qazi et al., 2017); as also demonstrated by the isotopic tracers in the upper Ganga catchment, where enhanced sediment supply in the recent historical times was attributed to catchment-scale deforestation (Wasson et al., 2008).

The present study attempts to understand the complex interactions between climate, anthropogenic and geomorphic processes during the mid-to-late Holocene by investigating the relict lake sediment and the flood deposits overlying the fluvial terraces in the upper Ganga catchment. Thus, the objectives of the study are to (i) reconstruct and ascertain the causes of millennial and centennial-scale (mid to late Holocene) climate variability, and (iii) explore the causes of floods with emphasis on the climate-fire-and human interactions.

## 2. Study area

The relict lake sediments are retrieved from a saucer-shaped Benital Lake (Pindar valley, upper Ganga catchment) and the flood sediments overlie the fluvial terraces in the lower Alaknanda valley (Fig. 1). The Alaknanda River originates from the Satopanth and Bhagirath-Kharak group of glaciers in the Chaukhamba massif (>6000 m asl). It flows for ~230 km before meeting the Bhagirathi River at Devprayag (450 m asl), from where onwards it is called the Ganga River (Fig. 1).

The total annual precipitation reconstructed using the past 30 years (1970–2000 CE) data from WorldClim V2 (~1 km resolution) (Fick and Hijmans, 2017) shows that the ISM contributes ~80% of precipitation during summer and post-monsoon season (June-September-November) (Fig. 2). The annual precipitation is < 1200 mm/year in the valley around Srinagar town and increases to >1500 mm/year on the southern mountain front (e.g., around Benital, Badanital). The orographic barrier is structurally represented by the Main Central Thrust (MCT). Following this, the rainfall gradually declines in the north (Fig. 2). Topography facilitates the uplift of warm-moist air masses on windward slopes which are cooled adiabatically resulting in increased relative humidity, cloud formation, and precipitation (Shrestha et al., 2012). During the summer season, cloudbursts leading to torrential rains are common in the vicinity of an abrupt rise in the relief such as the southern slopes (orographic barrier). The relief not only modulates the spatial distribution of precipitation but also governs the floristic composition, which ranges from the sub-tropical pine, Himalayan moist temperate, mixed conifer, to subalpine/alpine forest, and alpine meadows above the tree line in the catchment.

The Benital Lake (30°09′38″N and 79°014′45″E, 2500 m amsl) is nestled on a saddle, south of the MCT, and receives heavy convective rainfall during summer (Bhushan et al., 2018). The average annual temperature based on Climate Research Unit (CRU) dataset (1901–2017 CE) (https://crudata.uea.ac.uk/cru/data/hrg/) for the Pindar valley is ~14 °C. The lake is fed by the ISM precipitation through surface runoff and has a poorly defined drainage network (Fig. 3).

The lake catchment lithology comprises of slate, phyllite, and quartzite with occasional basic intrusive rocks (Bhushan et al., 2018 and reference therein). The poorly defined strand line indicates that the maximum area occupied by the lake was ~0.5 km$^2$. Presently, the lake has shrunk to a ~1–2 m deep puddle covered with aquatic grasses. The lake catchment vegetation is characterized by 60% woody (tree and shrub) and 40% non-woody (grass) plants. The woody plants are C3 type (e.g., *Desmodium, Rhododendron, Myrica, Prunus,* and *Pyrus*) and the non-woody plants are C4 type (Ghosh et al., 2020).

The flood sequences are preserved between Srinagar and Devprayag (lower Alaknanda valley) (Fig. 1). Around six asymmetrically paired fill terraces (T6 to T1) are preserved preferably along meandering loops of the Alaknanda River (Fig. 1) (30°12′–30°14′ N and 78°45′–78° 0′ E) (Juyal et al., 2010). The flood deposits overlying the terraces are variably incised by the seasonal streams. The vegetation is dominated by *Pinus roxhburghi* (1400–700 amsl), *Dalbergia sissoo*, and *Acacia* spp. (700 m) (Sundriyal et al., 2007).

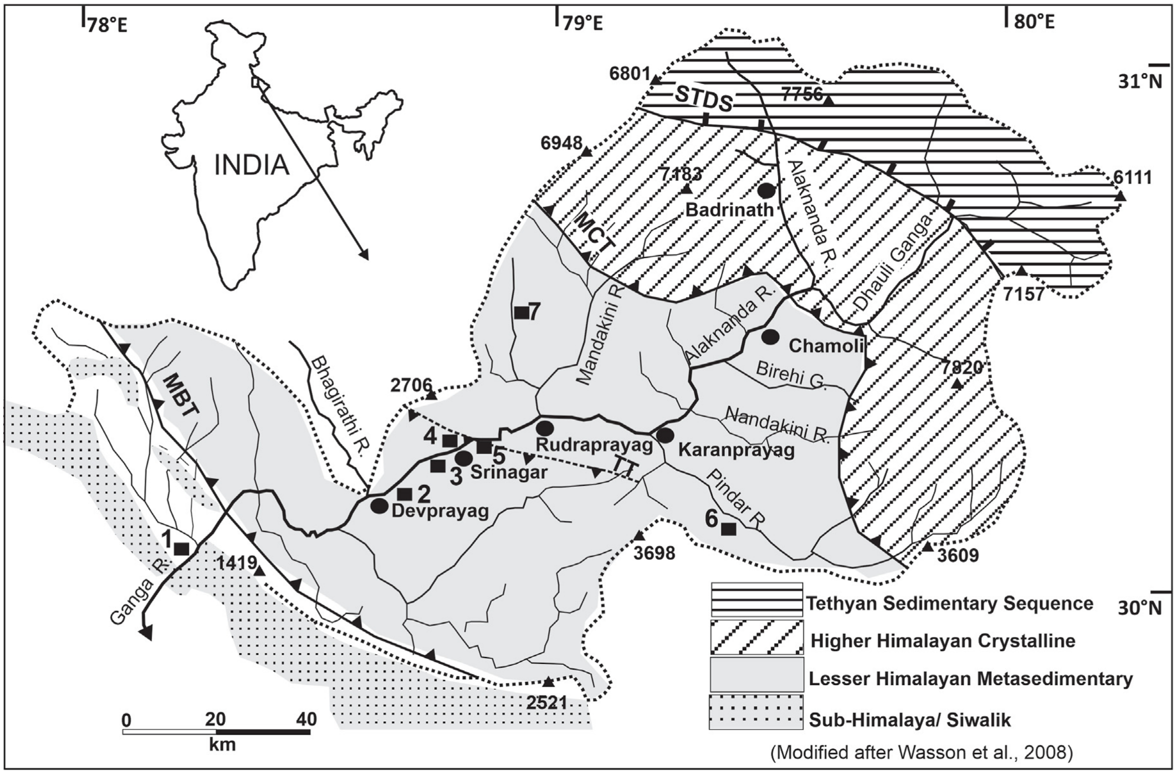


**Fig. 1.** Simplified geological and structural map of the Alaknanda valley (upper Ganga catchment). The locations discussed in the text are 1- Raiwala, 2- Devprayag, 3-Bhainswara, 4-Choras, 5-Swit, 6-Benital and 7- Badanital Lake. Flood deposits are located at 1–4. MBT- Main Boundary Thrust, TT- Tons Thrust, MCT- Main Central Thrust, STDS- South Tibetan Detachment System.

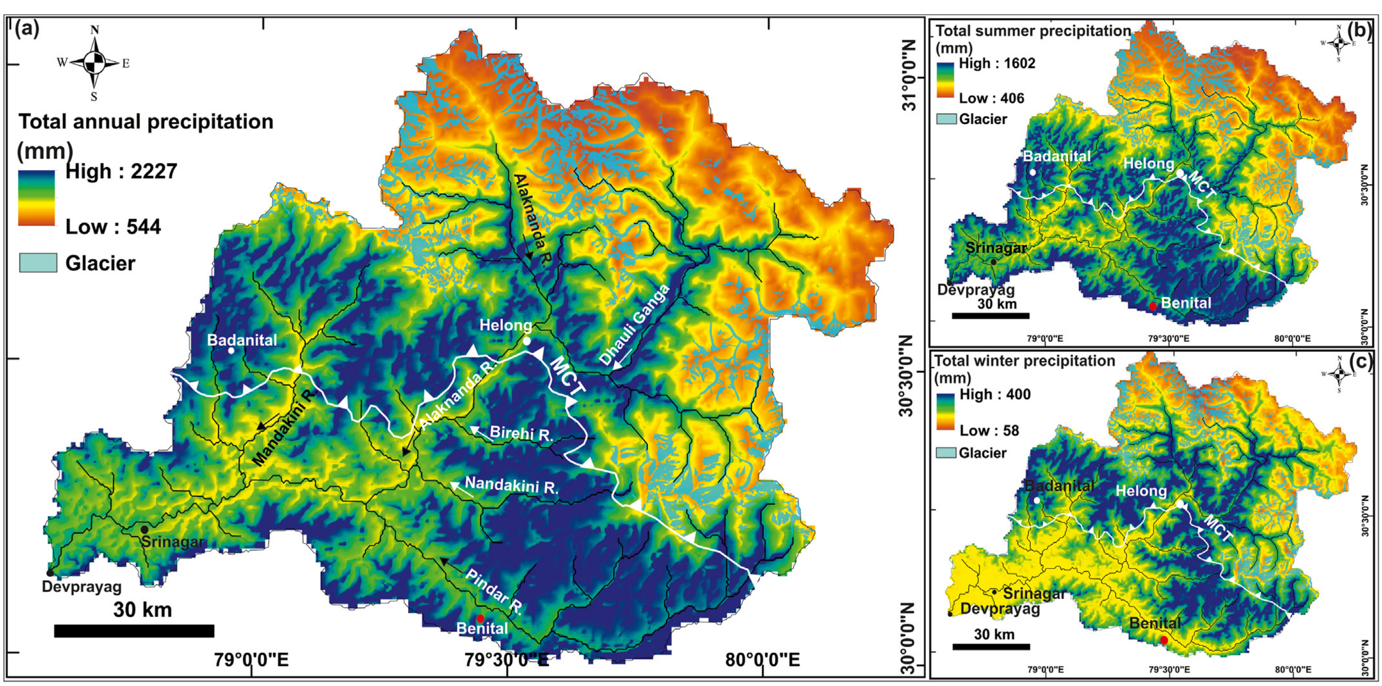


**Fig. 2.** The precipitation maps of the Alaknanda valley generated from average monthly datasets (1970–2000) showing (a) total annual (b) total summer (June–September) and (c) total winter (December–February) precipitation (in mm) (data source: www.worldclim.org, Fick and Hijmans, 2017). A well-defined precipitation gradient can be seen where the southern mountain front around the Main Central Thrust (MCT) receives the maximum precipitation. Benital relict lake location (red dot) and modern glaciers are also shown (blue). (For interpretation of the references to colour in this figure legend, the reader is referred to the Web version of this article.)

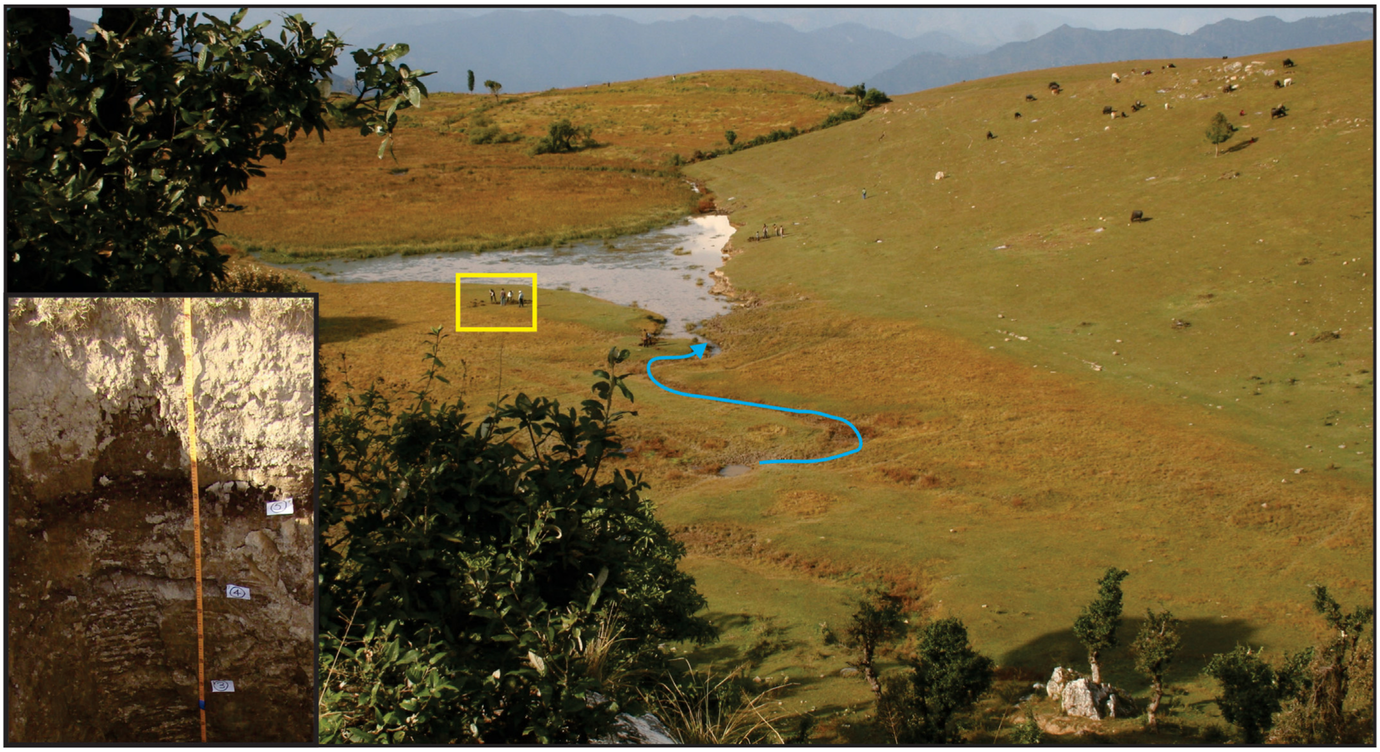

**Fig. 3.** Photograph of Benital Lake showing the sampling location (yellow rectangle). The blue line marks the seasonal channel feeding the lake. In the inset, photograph of the excavated profile. (For interpretation of the references to colour in this figure legend, the reader is referred to the Web version of this article.)

## 3. Methodology

To understand the mid-to-late Holocene climate variability vis-à-vis terrain response in terms of floods, forest fires, and anthropogenic influence, the Benital Lake sediments were analysed for environmental magnetism, major/trace element geochemistry, and the temporal changes in microcharcoal concentration. The extreme hydrological response is inferred from the chronologically constrained coarse to medium sand horizons (flood deposits) overlying the optically dated terrace sequences (Juyal et al., 2010; Ray and Srivastava, 2010).

### 3.1. Chronology

Three uncalibrated published (Bhushan et al., 2018) radiocarbon ages 1400 ± 109 years (70 cm from the surface), 3649 ± 65 years (90 cm), and 5520 ± 128 years (125 cm) are used for age-depth modelling after calibration with IntCal13 (Reimer et al., 2013). With IntCal20 (Reimer et al., 2020) the calibrated ages differ only by 0.6 ± 0.5% (Supplementary Table S1). To maintain consistency (and comparability) we are using IntCal13 calibrated ages after Bhushan et al. (2018). The modern age was constrained with −57 ± 5 years (2007 CE, sample collection year) at the depth of 2 cm from the modern surface. The ages were modelled to 125 cm depth for the proxy measurements. Due to low chronometric resolution between depths 2–70 cm, and 90–125 cm, the uncertainty is relatively higher for the modelled ages. The ages between 32.5 and 70 cm from the surface are extrapolated. Two age-depth models *Bchron* (Haslett and Parnell, 2008) and *rbacon* (Blaauw and Blaauw, 2021) using R-scripts (based on Bayesian statistics) were employed for comparison. Both age-depth models (using Markov Chain Monte Carlo iterations) yielded similar results for the mean ages. The modelled age range is 600 cal yr BP (0.6 ka) to 6000 cal yr BP (6.0 ka) at the 100-year interval (top 125 cm). Error in the interpolated ages was calculated using 25th and 75th percentiles values produced by *Bchron* within 1σ. The error was not calculated for the *rbacon* ages. Henceforth in the result and discussion, we will be using ka (kilo year) for ages. The parameters used for age-depth modelling are discussed in supplementary (Table S1).

For optical dating, sediment samples from coarse to medium sand on the upper terrace surfaces were collected in opaque metal pipes. The ages are obtained on quartz extract using the Single Aliquot Regeneration (SAR) technique. The quartz extraction procedure used is after Juyal et al. (2010). The equivalent dose (ED) and ages are calculated using R-script (Burow, 2019) and DRAC online (Durcan et al., 2015).

### 3.2. Geochemical proxies

The geochemical proxies in lake sediments may be used to infer temporal changes in climatically modulated surface runoff intensity (Haug et al., 2001; PAGES Hydro2k Consortium, 2017). In the present case, it may be linked to rainfall and/or snowmelt as well as anthropogenic intervention (Corella et al., 2016; Bhushan et al., 2018). For example, during periods of active erosion (unstable soils), the mass transport of unleached soils from the lake catchment increases the concentration of high base content (e.g., $Na_2O$ and $K_2O$) in the lake. Whereas, during the periods of catchment stability as the erosion progresses, lake sediments receive erosive material from deeply weathered soil profiles which have diminished base content (Mackereth, 1966). Hence, the temporal changes in $Na_2O$ and $K_2O$ concentration can be used as climate proxies (weathering and erosion) (Mackereth, 1966; Engstrom and Wright, 1984) with higher concentrations suggestive of increased erosion/run-off. Similarly, Sr coexists in Ca-bearing minerals, while Rb is enriched in the K-rich minerals (Dasch, 1969). The enhanced chemical (physical) weathering rates leads to an effective fractionation of Rb and Sr (Dasch, 1969; Chen et al., 1999), resulting in a significant increase (decrease) in Rb/Sr ratio in residual weathered sediments (Brass, 1975; Jin et al., 2001). As Ca-bearing minerals easily break down in comparison to K-bearing minerals, chemical weathering readily leaches Ca-Sr. Consequently, Sr passes into the solution and is transported into the lake, where it is preferentially incorporated in authigenic carbonates or adsorbed on organic matter surfaces (Chen et al., 1999). Thus, the lower ratio of Rb/Sr in lake sediments would represent enhanced chemical weathering in the catchment during warm/humid phases and vice versa (Jin et al., 2006). Zr/Ti is used as a grain size indicator in lake sediment as Zr is concentrated in coarser fractions (silt to fine sand), while Ti is typically enriched in clays (Haliuc et al., 2020). Thus, the temporal changes in Zr/Ti ration can be used to infer the changes in catchment erosive input of mineral subsoil erosion (Oldfield et al., 2003).

For the geochemical (major and trace element) analyses, 44 samples (at depth 123 to 32 cm) were dried at 80 °C to remove the moisture, then powdered and sieved through a 60-μm sieve. The finely powdered samples (~2.0 g) were mixed homogeneously with (0.5 g) wax binder in agate-pestle and mortar. The mixture was filled in the standard aluminium cups (37 mm) and then subjected to 150 kN pressure using a hydraulic press for a minute. The pellets prepared were subjected to X-ray fluorescence (XRF) spectrometry technique (Axios, from Panalytical limited). The analytical precision at 2 σ for major oxides is <5% and for the trace elements is <1% (Shukla, 2011). The reproducibility of the data is checked through routine analyses of the standards such as Nova-13, MAG-1, and SDO-1.

### 3.3. Environmental magnetism

The environmental magnetism in lake sediments such as magnetic susceptibility ($\chi$), frequency-dependent susceptibility ($\chi$fd), magneto-mineralogical S-ratio, hard isothermal remanent magnetization (HIRM), and anhysteretic remanent magnetization (ARM) are often used to infer the past climate and human-induced changes (Oldfield et al., 2003; Wu et al., 2015). The variations in saturation isothermal remanent magnetization (SIRM) reflect the magnetic mineral concentration given that the magnetic grain size and mineralogy remain relatively constant. Alternatively, it represents the relative concentration of remanence carrying magnetic minerals (ferrimagnetic and antiferromagnetic) within the lake sediment (Abrahamsen and Readman, 1987; Snowball and Thompson, 1990). Thus, the high value of SIRM may either be attributed to increased magnetic mineral input (caused by intensive erosion) or decreased organic input (either due to low productivity or poor preservation) because organic matter may dilute deposited magnetic minerals and vice-versa (Wang et al., 2001). The $\chi$fd is a key indicator of material derived from soil/weathered regolith and provides an estimate of ultra-fine super-paramagnetic, ferromagnetic particles, which are secondarily produced by weathering and pedogenesis (Verosub and Roberts, 1995; Basavaiah and Khadkikar, 2004). The S-ratio is widely used as a measure of relative quantification of higher (hematite) to lower coercivity (magnetite) magnetic minerals (Verosub and Roberts, 1995; Basavaiah and Khadkikar, 2004). The susceptibility of ARM ($\chi$ARM) depends on the concentration and composition of the ferrimagnetic grains size range discriminating in favour of small grains near the stable single-domain/superparamagnetic grain boundary (Turner, 1997). Whereas HIRM is used as a measure of the mass concentration of high coercivity magnetic minerals, e.g., hematite and goethite (Basavaiah and Khadkikar, 2004; Liu et al., 2012).

Magnetic susceptibility was measured using a KLY-2 Kappabridge (Agico, Brno) for 44 samples (at depth 123 to 32 cm). The $\chi$fd is calculated as $\chi_{fd}\% = [100(\chi_{lf}-\chi_{hf})/\chi_{lf}]$ from the susceptibility measurements at low frequency (0.47 kHz, $\chi_{lf}$) and high frequency (4.7 kHz, $\chi_{hf}$). The ARM and susceptibility of ARM ($\chi_{ARM}$) are produced by inducing an alternating magnetic field (usually 100 mT) along with a small, direct bias field of the order 0.05 mT (Turner, 1997). Magneto-mineralogic S-ratio is calculated by dividing the isothermal remanent magnetization (IRM) under a reverse field of 0.3 T by the SIRM at 1.5 T ($IRM_{-0.3T}/SIRM_{1.5T}$) (Bloemendal et al., 1992). The measurements were made using a 2G SQUID magnetometer and an MMPM9 pulse magnetizer. HIRM is also defined using a 300-mT cut-off field HIRM= $(SIRM + IRM_{-0.3T})/2$ (Robinson, 1986; Bloemendal et al., 1988). The 300-mT cut-off field is applied because in the case of high-coercivity hematite small IRM acquisition occurs below 300 mT whereas in low-coercivity magnetite complete acquisition of SIRM occurs below 300 mT (Basavaiah and Khadkikar, 2004; Roberts et al., 2020).

### 3.4. Micro-charcoal analyses

Charcoal is an inorganic carbon compound formed by incomplete combustion of organic material under reducing conditions and is transported to a lake by airborne (long-distance) and surficial processes (local) during a fire (Whitlock and Larsen, 2002; Conedera et al., 2009)¶. Usually, charcoal derived from plant material is black, opaque, and angular with an elongate-prismatic appearance with some cellular structures (Patterson et al., 1987; Enache and Cumming, 2006; Scott and Damblon, 2010). Thus, micro-charcoal is indicative of catchment-wide fires while macro-charcoal may represent local fires (Iglesias et al., 2015). Additionally, forest fires besides degrading the soil organic matter (top Ah horizon) (Dunnette et al., 2014; Sarangi et al., 2022) significantly affect the soil magnetic properties due to the processes of reduction followed by re-oxidation of iron-bearing minerals such as magnetite or maghemite (Leborgne, 1960). Gedye et al. (2000) found that samples affected by fire (determined by increased charcoal concentrations) contained higher concentrations of ferrimagnetic minerals, magnetic particles, and were enriched in ultrafine single domain (SD) particles. Similarly, post-fire catchment erosion is an important geomorphic process responsible for affecting the elemental composition of lacustrine sediments and catchment soils (Leys et al., 2016).

The fire history of Benital Lake is reconstructed by quantification of micro-charcoal on pollen slides (Clark, 1982; Whitlock and Larsen, 2002) using the point count method (PCM) of Clark (1982). This method is suitable for the quantification of micro-charcoal particles dispersed in the atmosphere/water through regional and local fire events. A total of 44 samples (depth 123 to 32 cm) were processed to extract pollen and microscopic charcoal. The standard pollen analytical technique of acetolysis using aceotysing mixture (9:1 acetic anhydride and concentrated sulphuric acid) was employed (Erdtman, 1943). The charcoal fragments and a minimum number of 256 pollen grains of terrestrial taxa were counted. The charcoal abundance is estimated by recording the number of hits on charcoal particles scored by a standard number of points on an eyepiece reticle during scans of a predetermined area of the slide. The surface area of microcharcoal on pollen slides was measured and photo-documented under a light microscope (BX-63) using a grid with 400 squares of 156 $mm^2$ surface area at 400× magnification. The PCM suggests that the ratio of the number of points intersecting a phase to the total number of points applied is proportional to the area of that phase. The microcharcoal concentration is calculated as, Charcoal concentration $(x)(\%) = C_x / L_x \times 100$

Where $x$ is the sample number for which charcoal concentration is calculated as a percentage; $C$ is the identified number of micro-charcoals; $L$ is the total pollen of terrestrial taxa. The concentration of micro-charcoal on a palynological slide can be expressed as a count or as an area for which particles that are less than 100 μm in diameter are counted (Clark and Royall, 1995).

## 4. Results

### 4.1. Lake stratigraphy

The present study focuses on the upper ~125 cm which covers the mid-to the late-Holocene period (6 and < 0.5 ka). Based on sediment texture and charcoal concentration variability five units are identified (Fig. 4). The lowermost Unit-I is ~60 cm thick, pale-yellow sticky clay containing dispersed charcoal which increases towards the upper part of Unit-I (only the top 5 cm is considered for the analyses). This is succeeded by ~30 cm thick, dark brown organic-rich clay, Unit-II with relative increase (compared to unit-I) in dispersed charcoal. This unit contains three distinct organic-rich layers. This is followed by ~30 cm thick clayey Unit-III containing two distinct dark brown organic-rich horizons with increasing concentrations of dispersed charcoal. The overlying ~30 cm thick Unit-IV is moderately compact, fractured, silty-clay containing dispersed charcoal horizon. Finally, the succession is terminated by the deposition of ~30 cm thick silty-clay containing modern rootlets and is anthropogenically modified (Unit-V) (Fig. 4). For environmental magnetism, geochemistry and micro-charcoal concentration estimation, samples were collected at 2 cm intervals from depths 32–123 cm (Bhushan et al., 2018).

### 4.2. Valley-fill terraces and flood deposits

The flood deposits are represented by coarse, poorly graded sandy facies overlying the valley-fill terrace surfaces (T6 to T1) and are preserved as discrete patches around Srinagar in the lower Alaknanda valley (Figs. 1, 5 and 6). The wide asymmetrical valley (sinuosity 1.4) carved out on fractured phyllite rocks has provided accommodation space for fluvial aggradation under channel wide setting (Juyal et al., 2010). The oldest terrace T6 overlies the phyllite basement as discrete patches abutting the mountain flank ~100 m above the valley floor and is optically dated between 18 and > 15 ka (Juyal et al., 2010) (Fig. 5). The younger terraces (T5 to T2) occur between 50 and 10 m above the valley floor and are dated between 15 and 8 ka (Juyal et al., 2010). The youngest terrace T1 is preserved around Srinagar ~6 m above the present-day river channel and comprises of alternating sandy-gravelly sediment, capped by 1970's Alaknanda flood sediments (Wasson et al., 2008, 2013).

Texturally, the flood facies are moderately weathered, coarse to medium massive sand, at times interspersed with or overlain by phyllite-dominated (source proximal) debris flows (Fig. 5 and 6). At Swit village, flood deposits are identified as uppermost 1–2 m thick moderately weathered sand overlying the T4 terrace gravel and succeeded by multiple debris flows (Fig. 6).

As discussed above, the geomorphological setting and textural attributes of the sandy flood facies suggest deposition under the channel widening setting having a low sinuosity. The intervening and overlying crudely imbricated phyllite-dominated lithoclasts (e.g., T4 at Choras and Swit) indicate deposition under the internal zone of channel expansion during high magnitude floods (Benito et al., 2003) as the velocity rapidly decreases in channel widening settings. Often the high magnitude floods are known to be associated with local slope activity (Benito et al., 2003) where angular lithoclast may be deposited by the local rills and gullies (T6; Fig. 6) or may form an erosional base (Swit; Fig. 6). The distal channel facies/overbank deposits are preferentially preserved after the abandonment of (gravel dominated) terrace surface when the river reaches its former position only during peak floods (Vandenberghe, 2015). These facies were earlier interpreted as overbank flood facies during the waning phase under low discharge (end of aggradation phase) rather than the peak flood flows (Juyal et al., 2010).

### 4.3. Chronology

The modelled age-depth profile for the relict lake was developed using R-scripts, *Bchron* (Haslett and Parnell, 2008) and *rbacon* (Blaauw and Blaauw, 2021) for the age range 6.0 to 0.6 ka at a 100-year interval (Fig. 7). The temporal changes in sedimentation rate calculated within the dated units show minor variability. Low (consistent) sedimentation rate is observed during 6 and 4 ka (avg.

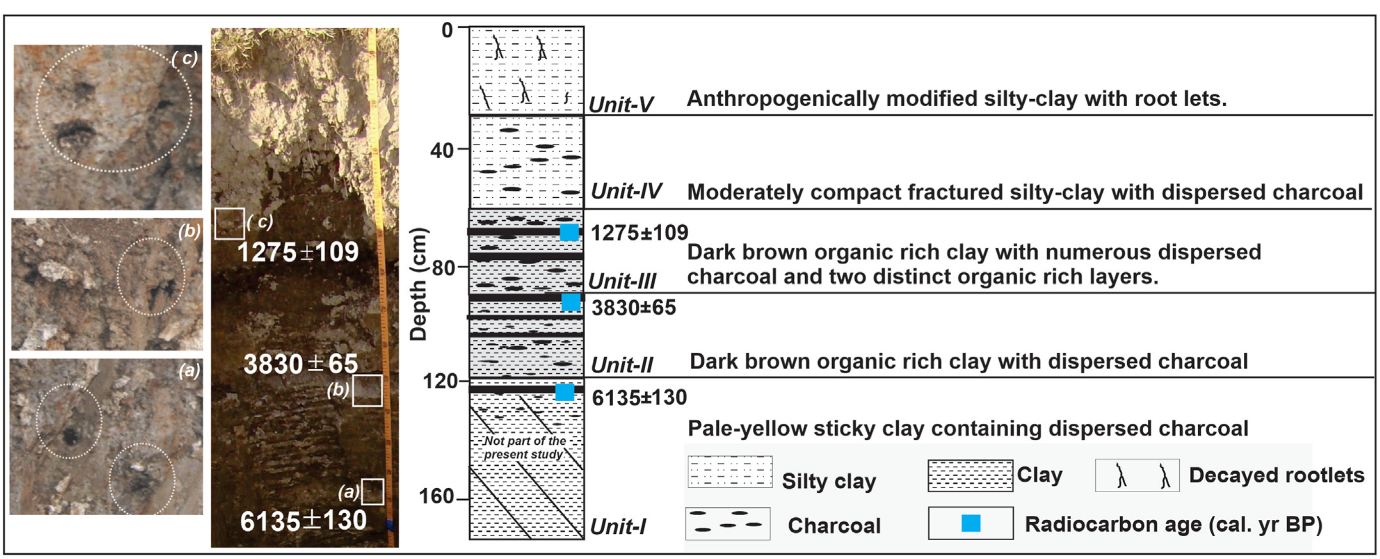


**Figure-4.** Relict Benital Lake stratigraphy with five distinct units containing organic-rich layers and dispersed macro-charcoal marked with white rectangles and shown in cropped insets (a to c). The section analysed is in between ~32 and 123 cm depth. The calibrated radiocarbon ages (in cal. yr BP) are from Bhushan et al. (2018).

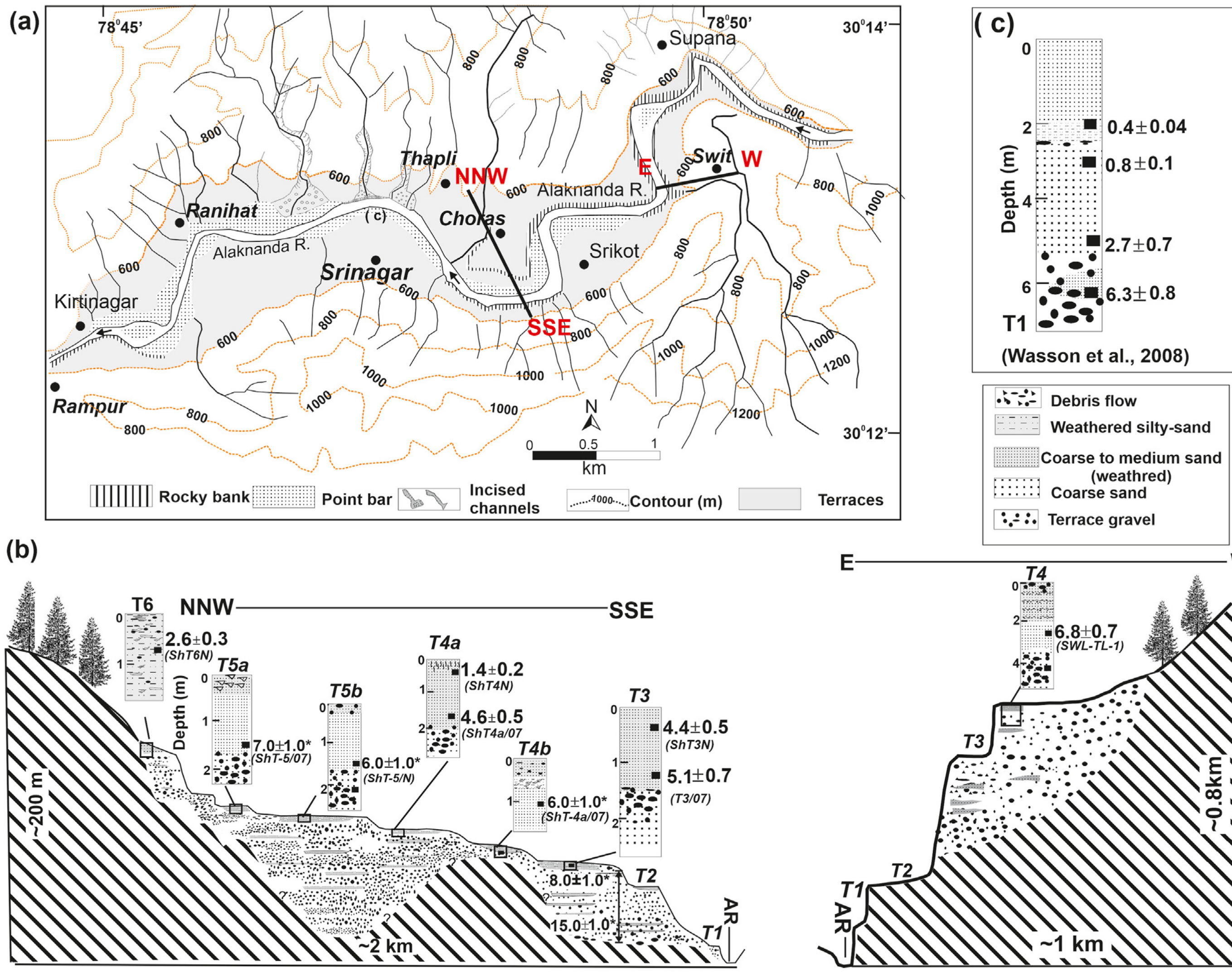


**Figure-5.** (a) The geomorphological map of the lower Alaknanda valley. The stratigraphy of the terraces and flood deposits in (b) is constructed along the cross-section profiles NNW-SSE and E-W (red lines). (b) The stratigraphy of the terraces and flood deposits around Choras (NNW-SSE) and Swit (E-W). Note that the fluvial aggradation occurred on common bedrock that was subsequently incised into six to four levels of terraces around Choras and Swit respectively. A broad stratigraphy of the flood sediments investigated are shown at their respective locations along with the optical chronology in kilo annum (ka). *After Juyal et al. (2010). (c) The composite stratigraphy and chronology of alluvial deposits (terrace T1) at Srinagar town (modified after Wasson et al., 2008). (For interpretation of the references to colour in this figure legend, the reader is referred to the Web version of this article.)

1.5 ± 0.2 cm/100 year) in comparison to a relatively high sedimentation rate (avg. 2.8 ± 1.6 cm/100 year) after 4 ka. (Supplementary Tables S2 and S3; Fig. 7).

The flood deposits at six locations are optically dated between 6.8 ± 0.7 and 1.4 ± 0.2 ka (Fig. 6; Table 1; Supplementary Fig. S1). The cumulative probability density function is used to infer the major flood phases from the new optical ages (Table 1) and the published data (Supplementary Tables S3 and S4). For the oldest records (~6.8 ka), the limited number of ages could be an artefact of preservation potential therefore, we have considered it as a flood phase despite low probability.

The termination of gravel facies for the valley fills is dated to 8 ± 1 ka (Juyal et al., 2010) while the oldest overbank flood deposits are dated to 6.8 ± 0.7 ka. After the major hiatus in sedimentation (~8.0 ka) river would have incised and eroded its sediments significantly. A lag of 2.9 ka can be suggested between the deposition of terrace gravel and the overlying sandy facies (flood deposit) that is calculated as gravel age plus error (8 + 1 = 9 ka) and overbank flood deposit age minus error (6.8-0.7 = 6.1 ka). The erosion rate around Srinagar (Lesser Himalaya) is estimated to be 0.8 ± 0.4 mm/year (Vance et al., 2003) implying that the riverbed (valley-fill terrace) was lowered by at least ~2 m (0.8 mm/yr x 2900 years) during the time of the oldest flood (6.8 ± 0.7 ka). This estimate, however, is the most conservative assuming the minimum rate of erosion and would have implications for the peak discharge required to overtop the gravel facies. Nevertheless, the youngest flood deposits dated to 1.4 ± 0.1 ka, suggest increasing peak discharge with time (Fig. 6; Table 1) during which the riverbed would have been lowered by ~6 m (by the conservative estimate) (Fig. 6; Table 1).

### 4.4. Geochemistry

Temporal changes in major and trace elements and their ratios in lake sediment represents the climatic changes that occur in the lake catchment. The concentration range varies for various

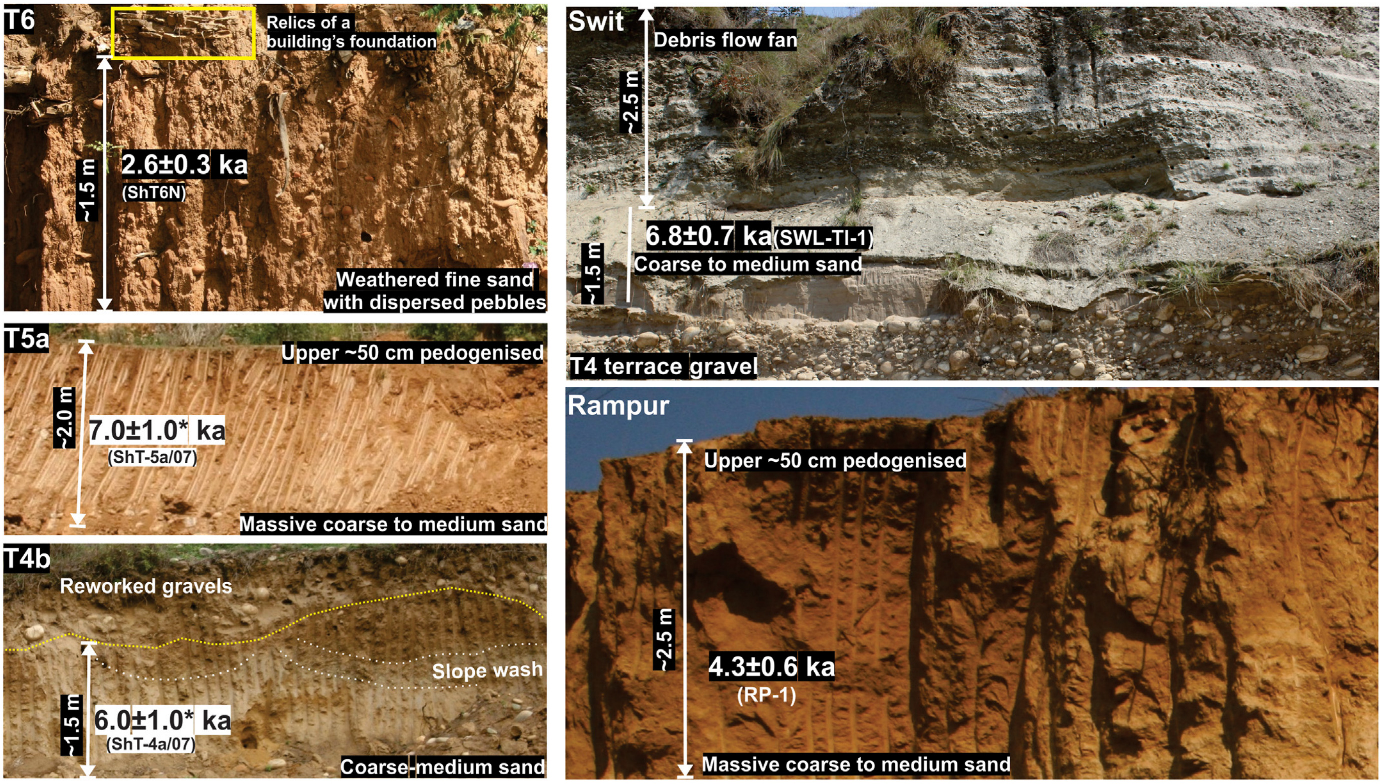


**Figure-6.** Field photographs of the flood deposits overlying the terraces around Srinagar (lower Alaknanda valley) at selected locations. These are represented by coarse to medium sand. Optical ages are also marked. *After Juyal et al. (2010).

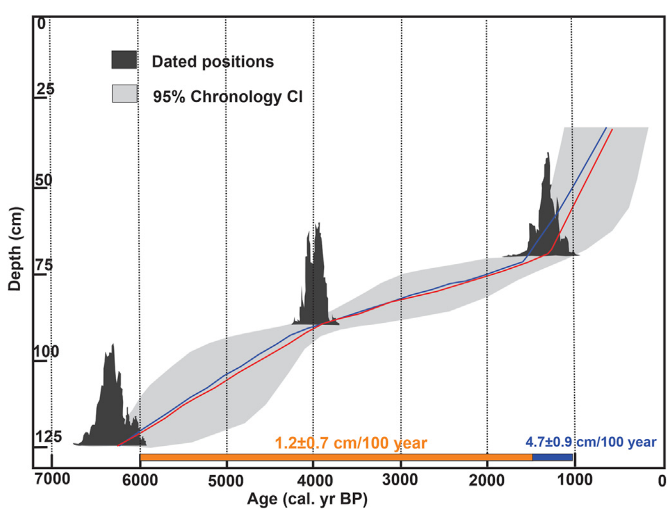


**Figure-7.** The age-depth modelling plot constructed using *Bchron* (blue line) (Haslett and Parnell, 2008) and *rbacon* (orange line) (Blaauw and Blaauw, 2021) post 6 ka at 95% confidence interval (CI) for top 125 cm. The average sedimentation rate is also shown (Supplementary Table S2). (For interpretation of the references to colour in this figure legend, the reader is referred to the Web version of this article.)

elements as - $Na_2O$ (0.41–1.1%), $K_2O$ (2.2–2.7%), Sr (75.3–96.6 ppm); Zr/Ti ratio ($160 \times 10^{-4}$ to $213 \times 10^{-4}$), and Rb/Sr ratio (1.58–1.84) (Fig. 8; Supplementary Table S5).

### 4.5. Environmental magnetism

The SIRM varies between 20.6 and 41.2; the $\chi$fd show significant change from 1.26 to 5.61; the $\chi$ARM fluctuates between 0.01 and 0.03; the magnetomineralogic S-ratio varies appreciably between 0.4 and 0.8, and the HIRM also show high variability (5.2–19.3) (Fig. 8; Supplementary Table S6).

### 4.6. Micro-charcoal

Lake sediments are excellent repositories of paleo-fire records as the evidence of fires is preserved in the form of micro and macro charcoal. The analysis of charcoal, along with sediment geochemistry and magnetic anomalies can be used to reconstruct the temporal changes in climate-fire linkages. Microcharcoal is usually scavenged by rainwater, transported (locally) by surface runoff, and incorporated into sediments after a long-distance aerial transport involving lifting by air. Compared to this, macro-charcoal is mostly transported by fluvial processes (e.g., surface runoff within the lake catchment) (Patterson III et al., 1987; Innes and Simmons, 2000). Thus, micro (macro) charcoal represents the catchment-wide (local) fires (Iglesias et al., 2015). Charcoal peaks in sediment cores may also result from taphonomic effects (i.e., erosional transport of charcoal residing in surface soils into the lake basin) (Cowart and Byrne, 2013). To circumvent it, the ratio between charcoal accumulation rates and pollen accumulation rates at each level was calculated in the section. Further, the amplitude/frequency of charcoal peaks in sediment may be modified by regional/local processes such as post-fire sediment accumulation (Innes and Simmons, 2000). However, relatively higher percentages of microcharcoal can be interpreted as prominent fire episodes without making a distinction between intensity/frequency intervals (Innes and Simmons, 2000). In Benital Lake, the peaks of micro-charcoal coinciding with increased concentration of visually observed macro-charcoal are used as an indication of enhanced forest fires

**Table 1**
Details of the equivalent dose (ED), overdispersion (OD), number of discs considered for age computation (n), radioactivity details (U, Th, K), dose rate (DR), and optical ages obtained for flood deposits (30°12′–30°14′N and 78°45′–78°50′E). The central age model (CAM) was used to calculate the ages as the OD is <40% (Galbraith et al., 1999, 2005).

| S. No. | Sample Name | ED ± Error (Gy) | OD (%) | n | U (ppm) | Th (ppm) | K (%) | DR (Gy/ka) | Age ± error (ka) |
|---|---|---|---|---|---|---|---|---|---|
| 1. | **ShT3N** | 20.91 ± 0.74 | 12 | 23 | 7.6 ± 1.2 | 22.6 ± 9.0 | 1.8 ± 0.1 | 4.81 ± 0.49 | 4.4 ± 0.5 |
| 2. | **ShT4N** | 6.37 ± 0.37 | 15 | 10 | 7.9 ± 1.0 | 18.7 ± 7.5 | 1.8 ± 0.1 | 4.63 ± 0.43 | 1.4 ± 0.2 |
| 3. | **ShT6N** | 11.35 ± 0.75 | 15 | 8 | 5.9 ± 1.1 | 17.6 ± 4.0 | 2.1 ± 0.1 | 4.41 ± 0.31 | 2.6 ± 0.3 |
| 4. | **SWL-TL-1** | 33.29 ± 2.16 | 30 | 25 | 5.0 ± 1.0 | 22.1 ± 5.3 | 2.5 ± 0.1 | 4.87 ± 0.36 | 6.8 ± 0.7 |
| 5. | **T4a/07** | 24.06 ± 1.42 | 26 | 24 | 4.9 ± 1.2 | 9.6 ± 4.0 | 1.2 ± 0.1 | 5.25 ± 0.46 | 4.6 ± 0.5 |
| 6. | **T3/07** | 27.30 ± 2.60 | 26 | 9 | 2.4 ± 0.5 | 4.3 ± 1.8 | 1.6 ± 0.1 | 5.39 ± 0.49 | 5.1 ± 0.7 |
| 7. | **RP-1** | 13.85 ± 1.52 | 19 | 4 | 3.6 ± 1.1 | 9.2 ± 3.8 | 1.9 ± 0.1 | 3.23 ± 0.28 | 4.3 ± 0.6 |
| 8. | **Dev-TL-1** | 25.65 ± 2.47 | 39 | 19 | 6.2 ± 1.0 | 15.0 ± 6.1 | 2.0 ± 0.1 | 4.23 ± 0.37 | 6.1 ± 0.8 |

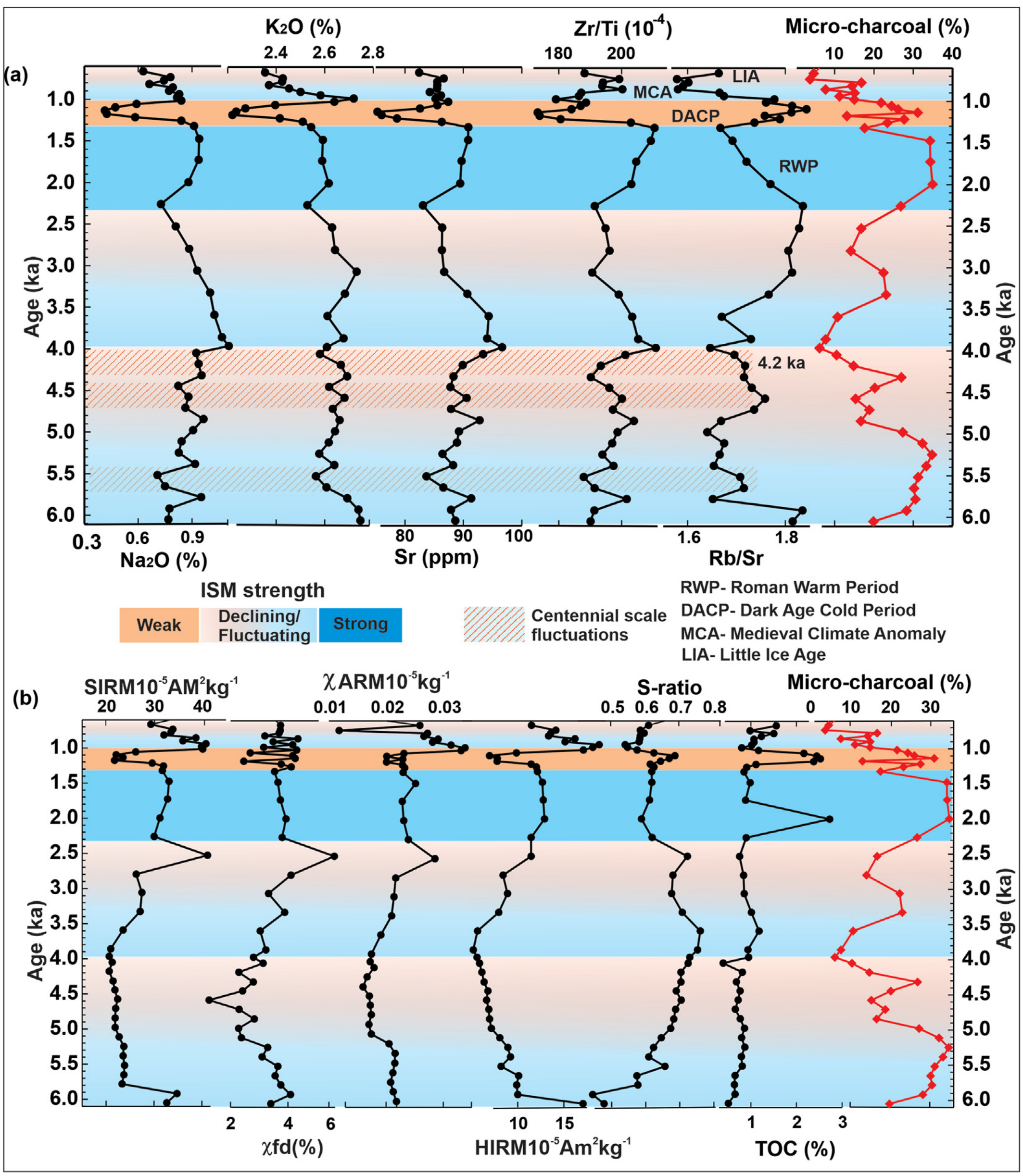


**Figure-8.** (a) The temporal changes in major/trace elements, and (b) the magnetic parameters used to infer the five climate phases (shaded stippling). The intensity of colours is used to represent the ISM strength as inferred in the text. In (a) the micro-charcoal concentration and the centennial-scale inversions known globally/regionally are also marked. Rb/Sr and TOC are after Bhushan et al. (2018). (For interpretation of the references to colour in this figure legend, the reader is referred to the Web version of this article.)

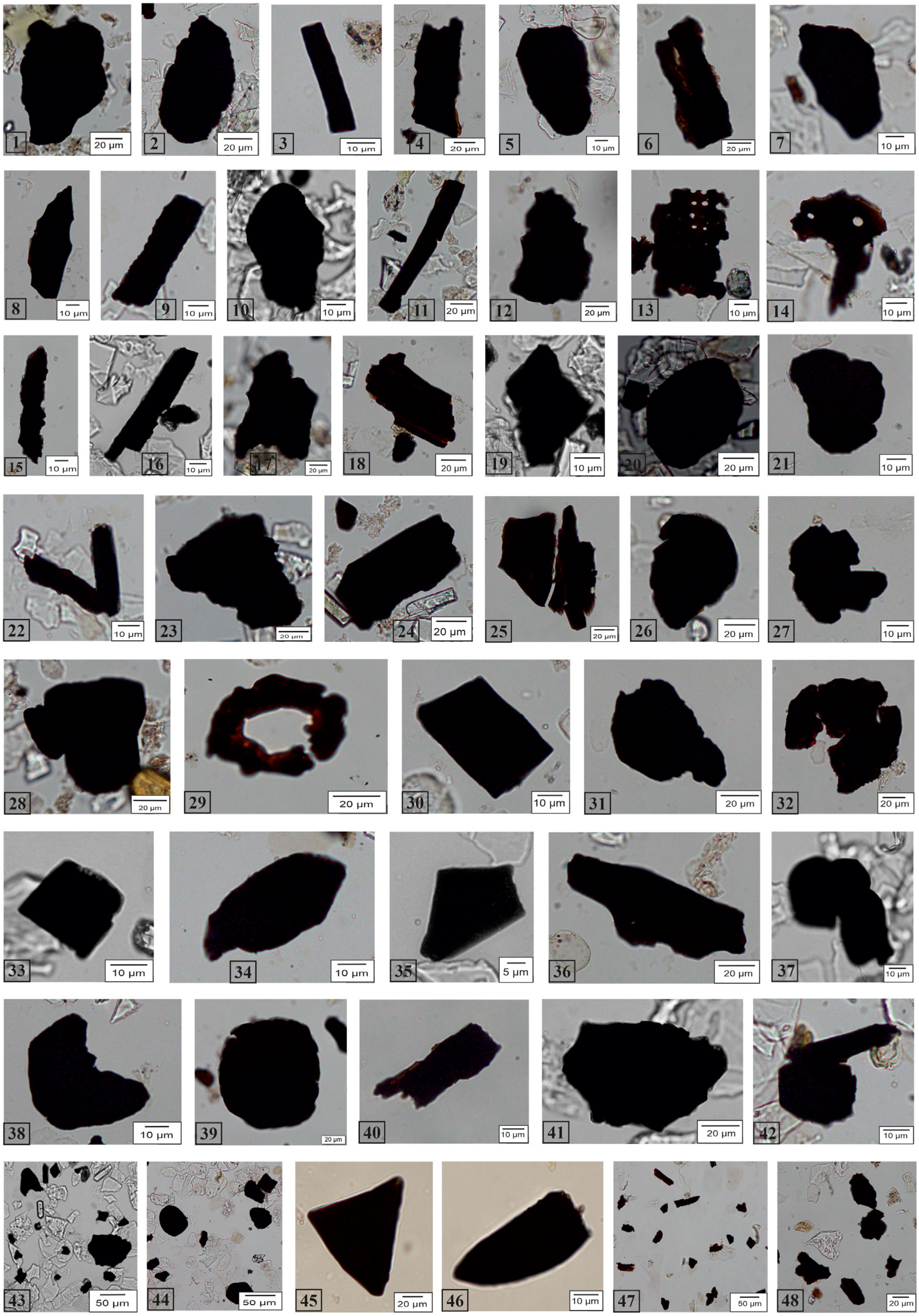


**Figure-9.** Photographs of charcoal morphotypes observed during microscopic analysis of Benital Lake sediments.

(Figs. 8 and 9). The micro-charcoal analysis shows variation from 4 to 35% in all stratigraphic units (Supplementary Table S5).

## 5. Discussion

We discuss the mid-to-late Holocene climate variability based on geochemical and magnetic proxies followed by the evidence of human occupation, and terrain response in terms of floods and forest fires. Finally, an effort is being made to understand the complex inter-relationship between these processes.

### 5.1. Climate variability

Five phases of millennial to centennial-scale climate variability are identified which broadly correspond with the trend inferred by Bhushan et al. (2018). However, given the low resolution of the chronology, we have avoided bracketing the centennial-scale variations into separate phases, except where the break-in trend is prominent. The reversals in climate variability become frequent (and prominent) after 2 ka as observed in other global data proxies (Fig. 8).

(i) *Phase-1 (6.0 to 4.0 ka):* The initial period till ~5.1 ka, is marked by fluctuations in an overall increasing trend with prominent centennial-scale reversals in $Na_2O$, $K_2O$, Sr, and Zr/Ti and decreasing Rb/Sr ratio (Fig. 8). The magnetic proxies SIRM, $\chi$fd, $\chi$ARM, and HIRM show decreasing tendency while S-ratio is marked by an increasing trend. This suggests weak physical and chemical weathering and low erosive potential under moderate and fluctuating ISM. The micro-charcoal concentration increased within this period and a higher concentration of macro-charcoal was observed in the field.

Thereafter, the most prominent centennial-scale reversal in the above-mentioned proxies and therefore, the inferred hydrological response, is observed between 4.5 and 4.0 ka (marked as a separate phase in Bhushan et al., 2018). The $Na_2O$, $K_2O$, Sr, and Zr/Ti fluctuate with the lowest concentrations between 4.7 and 4.2 ka suggesting low run-off (physical weathering). Low Sr but higher Rb/Sr ratio suggests weak chemical/physical weathering in the lake catchment (Fig. 8). The SIRM fluctuates within a small range with a declining trend. The $\chi$fd and $\chi$ARM ratios are low and suggest contribution from weakly developed soils/regolith from the lake catchment. This is further corroborated by a slight decrease in HIRM and an increasing trend in S-ratio (Fig. 8). Climatically, this phase is interpreted as low-intensity ISM with the globally marked arid phase of 4.2 ka when charcoal concentration spiked within the drier phase. The average sedimentation rate calculated is 1.5 ± 0.1 cm/100 years.

(ii) *Phase-2 (4.0 to 2.2 ka)*: The proxies $Na_2O$, Sr, $K_2O$, and Zr/Ti show a declining trend while Rb/Sr show an upward trend. Since the relative concentration of these proxies is higher than Phase-1; this phase is inferred to have relatively increased humidity with a continuously declining trend and minimal variability. Bhushan et al. (2018) inferred weak to moderate ISM during this period. The TOC concentration almost mimics the detrital proxies. On the other hand, the ferrimagnetic minerals SIRM, $\chi$fd, $\chi$ARM, S-ratio, and HIRM show an increasing trend (Fig. 8) suggesting higher erosion of antiferromagnetic minerals linked mainly to unweathered sedimentary rocks or subsoil (Dearing et al., 1986) under increased run-off. An overall low charcoal concentration is observed which increases after 3.5 ka.

Within this phase, the period between ~3.2 and ~2.2 ka is marked by a prominent decline in the ISM as characterized by the lowest concentrations of the proxies $Na_2O$, $K_2O$, Sr, and Zr/Ti ratio with a corresponding increasing trend of Rb/Sr ratio (Fig. 8). The magnetic proxies SIRM, $\chi$fd, $\chi$ARM, and HIRM show increasing tendency while S-ratio is marked by a declining trend. This suggests weak physical and chemical weathering and low erosive potential under weak ISM as also inferred in Bhushan et al. (2018). The micro charcoal concentration shows a rising trend after 3.5 ka with a small peak between 3.5 and 3 ka most likely in response to a drier climate. In the field, a prominent macro-charcoal horizon was also documented corresponding to this phase. The average sedimentation rate calculated is 0.8 ± 0.1 cm/100 years.

(iii) *Phase-3 (2.2-1.4 ka):* The centennial-scale phase is represented by a prominent higher concentration of $Na_2O$, $K_2O$, Sr, and Zr/Ti ratio with a corresponding sharp decline in Rb/Sr (Fig. 8). The magnetic proxies SIRM, and HIRM in magnetic mineralogy show a slight increase, but magnetic grain size represented by $\chi$fd and $\chi$ARM, and the magnetic mineralogical S ratio either show a marginal decrease or no change (Fig. 8). The sedimentation rate remains low (1.6 ± 1.6 cm/100 yr) which cannot be implicated for the observed increase in $Na_2O$, $K_2O$, Sr and a corresponding decrease in Rb/Sr. Instead, it indicates that the enhanced chemical weathering in the catchment was facilitated by the prevalence of relatively enhanced moisture and temperature conditions (strengthened ISM). An increase in charcoal concentration (during enhanced moisture) indicates that the forest fire was independent of climate, and it could be due to anthropogenic forest clearance. The average sedimentation rate calculated is 0.9 ± 0.7 cm/100 years.

(iv) *Phase-4 (1.4 to 1.0 ka):* The phase is represented by a prominent decrease in $Na_2O$, $K_2O$, Sr, and Zr/Ti ratio with a corresponding increase in Rb/Sr ratio (Fig. 8). A similar trend is observed in mineral magnetic parameters, for example, the SIRM, $\chi$fd, $\chi$ARM, and HIRM whereas, the S-ratio shows an increasing tendency. The pattern of the geochemical and magnetic proxies and the grain size variability indicate an abrupt decline in precipitation (weak ISM). The micro-charcoal concentration shows an overall increase under a drier climate. Macro-charcoal horizon was also observed for this phase in the field. The period was not recognized as a distinct phase in Bhushan et al. (2018) although the trend of the related detrital proxies is the same. The average sedimentation rate calculated is 4.7 ± 1.0 cm/100 years.

(v) *Phase-5 (<1.0 ka):* This is the terminal phase of lake sedimentation marked by a prominent peak in $Na_2O$, $K_2O$, Sr, and Zr/Ti with a corresponding decrease in Rb/Sr ratio (Fig. 8). The phase is succeeded by a marked drier phase at ~0.6 ka with all the proxies showing an inverse trend. The magnetic proxies also show a corresponding declining trend after the initial increase marking a break in trend from the preceding drier phase. The geochemical and magnetic proxies indicate relatively humid conditions which deteriorate at ~0.6 ka. The charcoal concentration decreases in response to more humid conditions. The average sedimentation rate calculated is 5.6 ± 0.2 cm/100 years.

The last 6 ka is considered equivalent to the “Subboreal” and “Subatlantic” chronozones (Nesje and Dahl, 1993) when the summer insolation in the Northern Hemisphere continuously declined (Marcott et al., 2013). The 6 to 5 ka period marks the end of the humid phase in the lower latitudes (Mayewski et al., 2004). However, climate variability in the Holocene period was suggested to be

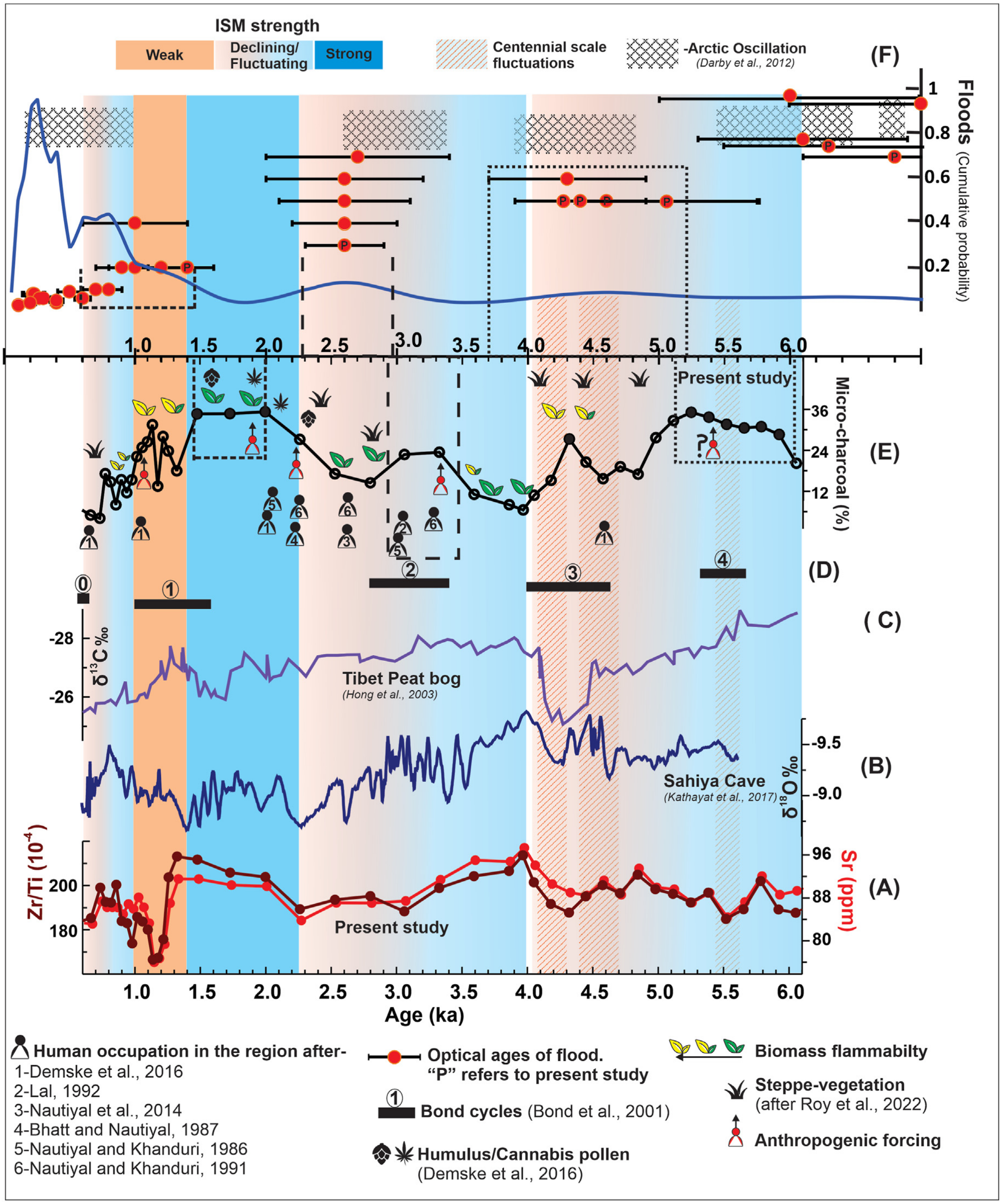


**Fig. 10.** **(A)** The geochemical proxies analysed in Benital Lake sediments show the inferred mid-to late Holocene climate variability and regional correlation with isotopic analyses of **(B)** Sahiya speleothem and **(C)** Hongyuan peat bog sequence, eastern Tibetan Plateau that is influenced by strong Indian summer monsoon (ISM) **(D)** The weak ISM phases are inferred to broadly correlate with the bond cycles (0–4). The dated archaeological and pollen evidence from published sources is represented to show anthropogenic influence in the upper Ganga valley. **(E)** The micro-charcoal data is plotted to infer the paleo-fire activity where solid circles represent macro-charcoal observed in the lake section. The vegetation type inferred from pollen (Demske et al., 2016; Roy et al., 2022) is interpreted for flammability of the biomass as well as human influence on the fire-climate dynamics. The anthropogenic forcing is inferred for the fire activity where either climate-vegetation-fire activity is decoupled or there is strong evidence of human influence. (?) indicates uncertainty in the anthropogenic forcings. Higher charcoal concentrations between 6 and 5 ka could have an anthropogenic role that cannot be established right now (due to lack of data). **(F)** The geomorphic response of the upper Ganga catchment to climate variability is inferred for floods from the cumulative probability curve and the optical ages in the present study and published data (Srivastava et al., 2008; Juyal et al., 2010; Wasson et al., 2008, 2013; supplementary; Tables S2 and S3). Note that floods cluster during weak/transient ISM and are suggested to be influenced by negative arctic oscillations inferred after Darby et al. (2012). The floods mostly occur after the peak forest fires suggesting greater sediment mobilization due to deforestation-induced erosion/surface runoff (suggested linked phases marked by dotted rectangles). These phases also broadly overlap with greater human influence. Nevertheless, the association of human-induced deforestation through forest burning remains suggestive and awaits more robust analyses.

quasi-periodic (O'Brien et al., 1995), when Bond et al. (1997, 2001) linked these 1500-year cycles (Bond cycles) to solar activity (equivalent to Dansgaard–Oeschger cycles) based on petrologic tracers of drift ice in the North Atlantic. The geochemical and magnetic proxies in the current study show synoptic scale synchroneity with the global millennial and centennial climate events. The centennial-scale relatively drier periods of lower ISM, marked by reduced catchment weathering and erosion show a close correspondence with bond cycles 0–4 (Fig. 10 D). The disruption of the North Atlantic thermohaline circulation leading to cooler sea surface temperature and thus, reduced land-sea thermal contrast has been invoked as a teleconnection between the north Atlantic and the ISM (e.g., Hong et al., 2003). Similarly, the relatively wetter phases seem to be a response to the increased sunspot activity (Solanki et al., 2004) during which the ISM is suggested to enhance by northward propagation of the inter-tropical convergence zone (ITCZ) forced by equatorial convective activity (weakened Brewer-Dobson circulation) (Kodera, 2004; Gupta et al., 2005).

Regionally, the phases inferred show a broad coherence with other archives in similar geomorphic settings on a millennial time scale (Fig. 10). For example, Srivastava et al. (2017) used the (a)biotic, and isotopic proxies on a peat deposit (NW of the Benital Lake in Kedarnath, upper Mandakini valley) infer warmer and wetter conditions at the beginning of Phase-1 (6.0-4.0 ka) till 5.4 ka and drier conditions thereafter. Within this moderate ISM phase, TC% and $\delta^{13}C$ proxies show prominent reversals at the centennial scale (e.g., 5.8 ka; 5.3-5.1 ka; 4.3-4.0 ka; Srivastava et al., 2017) as inferred in the Benital Lake. Similarly, pollen analyses of a kame terrace in Gangotri valley (Roy et al., 2022) and Badani Tal in Mandakini valley (Demske et al., 2016) suggest the dominance of moist taxa at the start of Phase-1. The $\delta^{18}O$ record from Sahiya cave speleothem (east of Benital Lake) suggests enhanced ISM till 4.5 ka (Kathayat et al., 2017) with a declining trend between 4.5 and 4.1 ka indicating short-term reversal towards weakened ISM (4.2 ka arid event) (Fig. 10 B). This period is marked by a marginal increase in steppe taxa (Roy et al., 2022) and a change towards open forests in the upper Ganga catchment (Demske et al., 2016). Phase-2 (4.0–2.2 ka) of Benital Lake is inferred to have moderate ISM but with a declining tendency as also seen in gradually enhancing values of $\delta^{18}O$ values of the Sahiya speleothem (Kathayat et al., 2017). Peat records show the most improved climate conditions within 3.8–3.0 ka (Srivastava et al., 2017) while a marginal increase (decrease) in moist (steppe) taxa is observed in Gangotri valley (Roy et al., 2022). A prominent decline in the ISM after ~3.0 ka is also reflected in $\delta^{18}O$ values of the Sahiya speleothem (Kathayat et al., 2017); the biotic and isotopic proxies in Kedarnath peat (Srivastava et al., 2017); and increased steppe taxa percentages (Roy et al., 2022). The centennial-scale sharp climate fluctuations after 2.2 ka inferred as Phase-3 (2.2–1.4 ka), 4 (1.4–1.0 ka), and 5 (<1.0 ka) correspond to the Roman Warm Period (RWP), Dark Age Cold Period (DACP), and Medieval Climate Anomaly (MCA) terminating with the Little Ice Age (LIA) (Figs. 8 and 10). These phases are not only well represented in the Central Himalayan records (Srivastava et al., 2017; Kathayat et al., 2017; Roy et al., 2022) but also from the monsoon-dominated Hongyuan peat bog, eastern Tibetan plateau (Hong et al., 2003) implying that even the centennial-scale ISM variability had regional character (Fig. 10 C).

### 5.2. *Evidence of human occupation*

The archaeological evidence, although limited, indicates prominent human occupation since ~3 ka. For example, the beginning of cultivation in the upper Ganga-Yamuna valley is suggested by Painted Grey Ware (PGW) of the early Iron age (first millennial BCE) (Lal, 1992). The occurrence of Himalayan pine (*P. Roxburghe*) at Jakhera (Central Ganga plain), is indicative of the migration of PGW culture into the upper Ganga catchment (Lal, 1992; Tewari, 2003). In the Satluj valley, cist burial indicates sedentary habitation since 2.6 ka (Nautiyal et al., 2014). Similarly, a cave burial site at Malari, upper Alaknanda catchment since ~2.2 ka (Bhatt and Nautiyal, 1987); discovery of black slipware/plain grey ware at Thapli, lower Alaknanda valley (Nautiyal, 1991) that is dated to 1200–300 BCE in the Ganga plain (Lal, 1992); and grey and fine red ware found from the excavation at Ranihat (right flank of Alaknanda River) with the antiquity of c. 600 BCE (Nautiyal, 1991) suggest early sedentary human occupation at least since ~3 ka. The archaeological evidence also suggests effective and homogeneous culture diffusion in the Trans-Himalayan region of Uttarakhand, Himachal Pradesh around the first-second millennium B.C. (Nautiyal and Khanduri, 1986).

Pollen-based evidence from Badanital Lake by Demske et al. (2016), also indicates a perceptible impact of anthropogenic intervention on the terrain at the end of the mid-Holocene. The *Cerealia* pollen—an indicator of agricultural activity along with forest clearance inferred from charcoal dated to ~4.6 ka, suggests an early sedentary population (Demske et al., 2016). Based on the pollen corresponding to *Chenopodiaceae* communities, cultivated plants (e.g., cereals, buckwheat, and hemp), and an increase in the abundance of charred particles, hornwort spores, and coprophilous fungi during the last 300 years indicate large-scale deforestation in the region (Demske et al., 2016).

### 5.3. *Forcing factors for forest fires (natural versus anthropogenic)*

Dendroecological studies suggest that changes in large-scale atmospheric circulation and seasonal weather patterns synchronize fire activity across regions by affecting the length of fire season and fuel (biomass) moisture content (Haberle and Ledru, 2001; Iglesias et al., 2015). The direct linkage between (drier) climate and (high) fires is strongly affected by vegetation feedback which may alter the influence of climate (Rupp et al., 2000; Higuera et al., 2009). Traits such as leaf area to volume ratio, fuel moisture content, time since leaf-fall, the chemistry of vegetation, and companion species all influence the intensity and duration of fires and makes the relationship more complex (e.g., Weir and Limb, 2013; Popović et al., 2021).

Benital Lake sediments show relatively higher micro-charcoal concentration and macro-charcoal specs during phase-1 (~5.9–5.3 and ~4.5–4.3 ka; Figs. 9 and 10). The increased $\delta D_{C29}$ and $\delta^{13}C$ of leaf wax lipid in Benital Lake sediment suggest an arid mid-late-Holocene period dominated by non-woody (C4) plants compared to the early Holocene (Ghosh et al., 2020). Pollen records from the upper Ganga catchment (Demske et al., 2016; Roy et al., 2022) show an increase in steppe-type vegetation and dominance of flammable vegetation such as *Alnus, Betula, Abies* and Rosaceae with less flammable *Quercus* between 4.5 and 4.0 ka and severe forest disturbance. We assert that fires ~4.5–4.3 ka was favoured by fluctuating ISM with overall drier conditions and an abundance of flammable material (Fig. 10 E). The anthropogenic influence may also have played a role as suggested by large-scale forest clearance (Demske et al., 2016). A relatively higher concentration of micro-charcoal is also observed at ~3.4–3.0, 2.0–1.5, and ~1.0 ka (Fig. 10 E) when climate-vegetation dynamics were unfavourable (e.g., the appearance of fire-resistant vegetation as *Caryophyllaceae*, *Diploxylon*) or humidity was relatively enhanced (Fig. 10 E). For <3 ka regional evidence of human interference is shown by the increase in *Humulus/Cannabis* pollen (Demske et al., 2016), and archaeological evidence (discussed above). Earlier similar studies have suggested a correlation between the Holocene population growth and increased fire activity (e.g., Black et al., 2006; Carcaillet et al., 2009; Vannière et al., 2011), particularly after a drier climate (Whitlock et al., 2010; Moritz et al., 2012; McWethy et al., 2013) as a transition in climate conditions favours a shift from hunting-gathering to pastoralism, farming, and industrialization (Pyne, 2001).

### 5.4. Geomorphic response

The optically dated flood records in the valley are clustered around ~6.5, 4.5, 2.6, 0.8, and 0.4 ka (Fig. 10 F) during relatively drier phases (Herzschuh, 2006) (Fig. 10). The Himalayan floods are suggested to be generated by multiple processes such as Glacial Lake Outburst Floods (GLOFs), and extreme precipitation events which often couple with temporary damning of the rivers by mass wasting (Wasson et al., 2008; Dimri et al., 2016; Sharma et al., 2017). The early Holocene outwash gravels overlying the relict proglacial lake sequences in the upper Ganga catchment may be attributed to GLOFs (Juyal et al., 2004, 2009; Sati et al., 2014; Rana et al., 2019).

During the mid to late Holocene glacial fluctuations were marginal in the upper Ganga catchment with glacial advances dated to 7.5-4.5, 3.4, and ~2 ka during weak ISM and cooler phases (Sati et al., 2014; Bisht et al., 2015; Rana et al., 2019). The marginal advances were punctuated by glacier recessions that represented mobilization/deposition of glaciofluvial terraces dated to ~5, ~3, and ~1 ka (Sati et al., 2014; Bisht et al., 2015). Sati et al. (2014) and Bisht et al. (2015) suggested increased slope activity (alluvial/scree fans) and associated impounding dated to ~3.6, 3.2, 3.4, and 2 ka in response to high rainfall events. Breaching of such temporary dams is also suggested as one of the dominant mechanisms for flood generation in the Himalayas (Wasson et al., 2008; Sharma et al., 2017). Climatically, the short-time scale climate reversals, corresponding to increased slope activity, are globally recognized and coincide with flood clusters in the study area (Fig. 10 F). In the Himalayas, and the mid-latitude regions, catastrophic floods are known to be generated under the weakened ISM conditions with the coupling of moisture-laden ISM and southward-penetrating, upper-level westerly troughs through Rossby wave breaking (Rasmussen and Houze, 2012; Sharma et al., 2017) as observed during the June 2013 devastating Uttarakhand flood (Vellore et al., 2016). These events are suggested to be regionally synchronized and controlled by ocean-atmosphere dynamics in the Northern Atlantic as the polar front migrates (Lowe and Walker, 2014; Benito et al., 2015; Vellore et al., 2016) during negative Arctic Oscillation (Darby et al., 2012).

The probability density peaks of the flood clusters succeed the relatively higher micro-charcoal concentrations (Fig. 10 E and F) which are indicative of degraded forests/deforestation (discussed in 5.3). Certainly, the relationship between land cover, erosion, and hydrology is complex and varied both spatially and temporally (Bradshaw et al., 2007; Wasson et al., 2008; Chaudhary et al., 2016). However, following deforestation, the severity of floods is known to increase by sediment bulking as the destabilized slopes are eroded (Gentry and Lopez-Parodi, 1980; Fitzpatrick and Knox, 2000). The degraded forest canopy reduces the rainfall interception, infiltration, and evapotranspiration which leads to higher surface runoff and thus, may amplify the impact of floods (Haigh, 1984; Bird et al., 2019). Such anthropogenically induced flooding caused by large-scale deforestation was observed during the 1970's Alaknanda flood (considered to be the largest flood in the 20th century) in the upper Ganga catchment (Kimothi and Juyal, 1996; Wasson et al., 2008). Although subject to further validation, the human intervention (deforestation and forest fires) cannot be ignored for the observed flood clusters since 3 ka.

## 6. Conclusions

The study demonstrates that the mid-to-late Holocene climate variability in the upper Ganga catchment was marked by millennial to centennial-scale climate reversals. The geochemical and magnetic proxies indicate minor fluctuations in overall moderate to weak ISM where the cooler and relatively drier phases are in sync with the North Atlantic climate perturbations.

The geomorphic response of the terrain to millennial-centennial scale climate variability is expressed by the glacial and glacio-fluvial landforms. The floods in the valley occur in relatively drier phases and were associated with impoundings caused by enhanced slope activity (alluvial/scree fans) during extreme precipitation events. We envisage that these events were triggered by an interaction between warm-humid monsoon and cold-dry westerlies through Rossby wave breaking particularly during negative Arctic Oscillation. The flood clusters succeed the prominent forest fires, and it is speculatively argued that the contribution of enhanced erosion and surface runoff due to deforestation could have amplified the floods, particularly after ~3 ka.

The forest fires in the catchment seem to be largely dictated by climate-vegetation feedback with a drier climate and flammable species as favourable factors. However, the coinciding evidence of permanent human settlement in the region makes anthropogenic forcing a very likely possibility, especially under unfavourable climate-vegetation feedback. The complex relationships explored here have the potential for more robust quantification in future.

## Individual contributions of each co-author

Shubhra Sharma and S.P. Sati conceived the idea, were involved in fieldwork, prepared figures, and wrote the manuscript with inputs from all the authors. Specifically, Shubhra Sharma did the optical ages; environmental magnetism was done by N. Basavaiah; Shilpa Pandey did the charcoal analysis; Y.P. Sundriyal and Naresh Rana were involved in fieldwork and discussion; Priyanka Singh did age-depth modelling; Subhendu Pradhan contributed in optical data presentation and climate data extraction; A.D Shukla and Ravi Bhushan did geochemical analysis; Rakesh Bhatt contributed in archaeology, and Navin Juyal was involved in the discussion.

## Declaration of competing interest

The authors declare that they have no known competing financial interests or personal relationships that could have appeared to influence the work reported in this paper.

## Data availability

Data will be made available on request.

## Acknowledgements

Authors are grateful to the two anonymous reviewers and the editor for sparing time to provide suggestions which immensely helped improve the manuscript. This work was carried out under DST/INSPIRE/04/2017/001289, Inspire Faculty Project, Department of Science & Technology, Govt. of India awarded to Shubhra Sharma. SP Sati acknowledges MoES/P.O. (Geo)/95/2017 for financial support in field. Shilpa Pandey is thankful to the Director, BSIP, for permission to carry out pollen and charcoal studies.

## Appendix A. Supplementary data

Supplementary data to this article can be found online at https://doi.org/10.1016/j.quascirev.2022.107725.

## References


Abrahamsen, N., Readman, P.W., 1987. Quaternary magnetostratigraphy in Denmark. Boreas 16 (4), 373–380.

Basavaiah, N., Khadkikar, A.S., 2004. Environmental Magnetism and its Application towards Palaeomonsoon Reconstruction.

Benito, G., Macklin, M.G., Panin, A., Rossato, S., Fontana, A., Jones, A.F., Machado, M.J., Matlakhova, E., Mozzi, P., Zielhofer, C., 2015. Recurring flood distribution patterns related to short-term Holocene climatic variability. Sci. Rep. 5 (1), 1–8.

Benito, G., Sánchez-Moya, Y., Sopeña, A., 2003. Sedimentology of high-stage flood deposits of the Tagus River, Central Spain. Sediment. Geol. 157 (1), 107–132.

Bhatt, R.C., Nautiyal, K.P., 1987. Trans-Himalayan Burials, Vis-À-Vis Malari. An Assessment. JOHSARD, pp. 11–12.

Bhushan, R., Sati, S.P., Rana, N., Shukla, A.D., Mazumdar, A.S., Juyal, N., 2018. High-resolution millennial and centennial scale Holocene monsoon variability in the Higher Central Himalayas. Palaeogeogr. Palaeoclimatol. Palaeoecol. 489, 95–104.

Bird, B.W., Barr, R.C., Commerford, J., Gilhooly III, W.P., Wilson, J.J., Finney, B., McLauchlan, K., Monaghan, G.W., 2019. Late-Holocene floodplain development, land-use, and hydroclimate–flood relationships on the lower Ohio River, US. Holocene 29 (12), 1856–1870.

Bisht, P., Ali, S.N., Shukla, A.D., Negi, S., Sundriyal, Y.P., Yadava, M.G., Juyal, N., 2015. Chronology of late Quaternary glaciation and landform evolution in the upper Dhauliganga valley, (Trans Himalaya), Uttarakhand, India. Quat. Sci. Rev. 129, 147–162.

Blaauw, M., Blaauw, M.M., 2021. Package 'IntCal'.

Black, M.P., Mooney, S.D., Martin, H.A., 2006. A> 43,000-year vegetation and fire history from lake Baraba, new south Wales, Australia. Quat. Sci. Rev. 25 (21), 3003–3016.

Bloemendal, J., King, J.W., Hall, F.R., Doh, S.J., 1992. Rock magnetism of Late Neogene and Pleistocene deep-sea sediments: relationship to sediment source, diagenetic processes, and sediment lithology. J. Geophys. Res. Solid Earth 97 (B4), 4361–4375.

Bloemendal, J., Lamb, B., King, J., 1988. Paleoenvironmental implications of rock-magnetic properties of Late Quaternary sediment cores from the eastern equatorial Atlantic. Paleoceanography 3 (1), 61–87.

Bond, G., Kromer, B., Beer, J., Muscheler, R., Evans, M.N., Showers, W., Hoffmann, S., Lotti-Bond, R., Hajdas, I., Bonani, G., 2001. Persistent solar influence on north Atlantic climate during the Holocene. Science 294 (5549), 2130–2136.

Bond, G., Showers, W., Cheseby, M., Lotti, R., Almasi, P., DeMenocal, P., Priore, P., Cullen, H., Hajdas, I., Bonani, G., 1997. A pervasive millennial-scale cycle in North Atlantic Holocene and glacial climates. Science 278 (5341), 1257–1266.

Bowman, D.M., Balch, J., Artaxo, P., Bond, W.J., Cochrane, M.A., D'antonio, C.M., DeFries, R., Johnston, F.H., Keeley, J.E., Krawchuk, M.A., Kull, C.A., 2011. The human dimension of fire regimes on Earth. J. Biogeogr. 38 (12), 2223–2236.

Bradshaw, C.J., Sodhi, N.S., Peh, K.S.H., Brook, B.W., 2007. Global evidence that deforestation amplifies flood risk and severity in the developing world. Global Change Biol. 13 (11), 2379–2395.

Brass, G.W., 1975. The effect of weathering on the distribution of strontium isotopes in weathering profiles. Geochem. Cosmochim. Acta 39 (12), 1647–1653.

Burow, C., 2019. calc_CentralDose: apply the central age model (CAM) after Galbraith et al. (1999) to a given De distribution. Function version 1.4.0. In: Kreutzer, S., Burow, C., Dietze, M., Fuchs, M.C., Schmidt, C., Fischer, M., Friedrich, J. (Eds.), Luminescence: Comprehensive Luminescence Dating Data Analysis. R Package Version 0.9.5. https://CRAN.R-project.org/package=Luminescence.

Carcaillet, C., Ali, A.A., Blarquez, O., Genries, A., Mourier, B., Bremond, L., 2009. Spatial variability of fire history in subalpine forests: from natural to cultural regimes. Ecoscience 16 (1), 1–12.

Chaudhary, R.P., Uprety, Y., Rimal, S.K., 2016. Deforestation in Nepal: causes, consequences and responses. Biol. Environ. Hazards Risks Disasters 335–372.

Chen, J., An, Z., Head, J., 1999. Variation of Rb/Sr ratios in the loess-paleosol sequences of central China during the last 130,000 years and their implications for monsoon paleoclimatology. Quat. Res. 51 (3), 215–219.

Clark, J.S., Royall, P.D., 1995. Particle-size evidence for source areas of charcoal accumulation in late Holocene sediments of eastern North American lakes. Quat. Res. 43 (1), 80–89.

Clark, R.L., 1982. Point count estimation of charcoal in pollen preparations and thin sections of sediments. Pollen et spores.

Clemens, S.C., Prell, W.L., 2007. The timing of orbital-scale Indian monsoon changes. Quat. Sci. Rev. 26 (3–4), 275–278.

Conedera, M., Tinner, W., Neff, C., Meurer, M., Dickens, A.F., Krebs, P., 2009. Reconstructing past fire regimes: methods, applications, and relevance to fire management and conservation. Quat. Sci. Rev. 28 (5), 555–576.

Corella, J.P., Valero-Garcés, B.L., Vicente- Serrano, S.M., Brauer, A., Benito, G., 2016. Three millennia of heavy rainfalls in Western Mediterranean: frequency, seasonality and atmospheric drivers. Sci. Rep. 6 (1), 1–11.

Cowart, A., Byrne, R., 2013. A paleolimnological record of late Holocene vegetation change from the central California coast. Calif. Archaeol. 5 (2), 337–352.

Darby, D.A., Ortiz, J.D., Grosch, C.E., Lund, S.P., 2012. 1,500-year cycle in the Arctic Oscillation identified in Holocene Arctic sea-ice drift. Nat. Geosci. 5 (12), 897–900.

Dasch, E.J., 1969. Strontium isotopes in weathering profiles, deep-sea sediments, and sedimentary rocks. Geochem. Cosmochim. Acta 33 (12), 1521–1552.

Dearing, J.A., Morton, R.I., Price, T.W., Foster, I.D.L., 1986. Tracing movements of topsoil by magnetic measurements: two case studies. Phys. Earth Planet. In. 42 (1), 93–104.

Demske, D., Tarasov, P.E., Leipe, C., Kotlia, B.S., Joshi, L.M., Long, T., 2016. Record of vegetation, climate change, human impact and retting of hemp in Garhwal Himalaya (India) during the past 4600 years. Holocene 26 (10), 1661–1675.

Dietze, E., Theuerkauf, M., Bloom, K., Brauer, A., Dörfler, W., Feeser, I., Feurdean, A., Gedminienė, L., Giesecke, T., Jahns, S., Karpińska-Kołaczek, M., 2018. Holocene fire activity during low-natural flammability periods reveals scale-dependent cultural human-fire relationships in Europe. Quat. Sci. Rev. 201, 44–56.

Dimri, A.P., Thayyen, R.J., Kibler, K., Stanton, A., Jain, S.K., Tullos, D., Singh, V.P., 2016. A review of atmospheric and land surface processes with emphasis on flood generation in the Southern Himalayan rivers. Sci. Total Environ. 556, 98–115.

Dunnette, P.V., Higuera, P.E., McLauchlan, K.K., Derr, K.M., Briles, C.E., Keefe, M.H., 2014. Biogeochemical impacts of wildfires over four millennia in a Rocky Mountain subalpine watershed. New Phytol. 203 (3), 900–912.

Durcan, J.A., King, G.E., Duller, G.A., 2015. DRAC: dose rate and age calculator for trapped charge dating. Quat. Geochronol. 28, 54–61.

Enache, M.D., Cumming, B.F., 2006. Tracking recorded fires using charcoal morphology from the sedimentary sequence of Prosser Lake, British Columbia (Canada). Quat. Res. 65 (2), 282–292.

Engstrom, D.R., Wright Jr., H.E., 1984. Chemical stratigraphy of lake sediments as a record of environmental change. In: Haworth, E.Y., Lund, J.W. (Eds.), Lake Sediments and Environmental History. University of Minnesota Press, Minneapolis, MN, pp. 11–67.

Erdtman, G., 1943. An Introduction to Pollen Analysis. Chronica Botanica, Waltham Mass (USA).

Fick, S.E., Hijmans, R.J., 2017. WorldClim 2: new 1-km spatial resolution climate surfaces for global land areas. Int. J. Climatol. 37 (12), 4302–4315.

Fitzpatrick, F.A., Knox, J.C., 2000. Spatial and temporal sensitivity of hydrogeomorphic response and recovery to deforestation, agriculture, and floods. Phys. Geogr. 21 (2), 89–108.

Galbraith, R.F., Roberts, R.G., Laslett, G.M., Yoshida, H., Olley, J.M., 1999. Optical dating of single and multiple grains of quartz from Jinmium rock shelter, northern Australia: Part I, experimental design and statistical models. Archaeometry 41 (2), 339–364.

Galbraith, R.F., Roberts, R.G., Yoshida, H., 2005. Error variation in OSL palaeodose estimates from single aliquots of quartz: a factorial experiment. Radiat. Meas. 39 (3), 289–307.

Gedye, S.J., Jones, R.T., Tinner, W., Ammann, B., Oldfield, F., 2000. The use of mineral magnetism in the reconstruction of fire history: a case study from Lago di Origlio, Swiss Alps. Palaeogeogr. Palaeoclimatol. Palaeoecol. 164 (1), 101–110.

Gentry, A.H., Lopez-Parodi, J., 1980. Deforestation and increased flooding of the upper Amazon. Science 210 (4476), 1354–1356.

Ghosh, S., Sanyal, P., Roy, S., Bhushan, R., Sati, S.P., Philippe, A., Juyal, N., 2020. Early Holocene Indian summer monsoon and its impact on vegetation in the Central Himalaya: insight from δD and δ13C values of leaf wax lipid. Holocene 30 (7), 1063–1074.

Gupta, A.K., Das, M., Anderson, D.M., 2005. Solar influence on the Indian summer monsoon during the Holocene. Geophys. Res. Lett. 32 (17), 1–4.

Haberle, S.G., Ledru, M.P., 2001. Correlations among charcoal records of fires from the past 16,000 years in Indonesia, Papua New Guinea, and Central and South America. Quat. Res. 55 (1), 97–104.

Haigh, M., 1984. Deforestation and disaster in northern India. Land Use Pol. 1 (3), 187–198.

Haliuc, A., Buczkó, K., Hutchinson, S.M., Ács, É., Magyari, E.K., Korponai, J., Begy, R.C., Vasilache, D., Zak, M., Veres, D., 2020. Climate and land-use as the main drivers of recent environmental change in a mid-altitude mountain lake, Romanian Carpathians. PLoS One 15 (10), e0239209.

Haslett, J., Parnell, A., 2008. A simple monotone process with application to radiocarbon-dated depth chronologies. J. Roy. Stat. Soc.: Ser. C (Appl. Stat.) 57 (4), 399–418.

Haug, G.H., Hughen, K.A., Sigman, D.M., Peterson, L.C., Rohl, U., 2001. Southward migration of the intertropical convergence zone through the Holocene. Science 293 (5533), 1304–1308.

Herzschuh, U., 2006. Palaeo-moisture evolution in monsoonal Central Asia during the last 50,000 years. Quat. Sci. Rev. 25 (1–2), 163–178.

Higuera, P.E., Brubaker, L.B., Anderson, P.M., Hu, F.S., Brown, T.A., 2009. Vegetation mediated the impacts of postglacial climate change on fire regimes in the south-central Brooks Range, Alaska. Ecol. Monogr. 79 (2), 201–219.

Hong, Y.T., Hong, B., Lin, Q.H., Zhu, Y.X., Shibata, Y., Hirota, M., Uchida, M., Leng, X.T., Jiang, H.B., Xu, H., Wang, H., 2003. Correlation between Indian ocean summer monsoon and north Atlantic climate during the Holocene. Earth Planet Sci. Lett. 211 (3–4), 371–380.

Iglesias, V., Yospin, G.I., Whitlock, C., 2015. Reconstruction of fire regimes through integrated paleoecological proxy data and ecological modeling. Front. Plant Sci. 5, 785.
Innes, J.B., Simmons, I.G., 2000. Mid-holocene charcoal stratigraphy, fire history and palaeoecology at North Gill, North York Moors, UK. Palaeogeogr. Palaeoclimatol. Palaeoecol. 164 (1), 151–165.
Jaffé, R., Ding, Y., Niggemann, J., Vähätalo, A.V., Stubbins, A., Spencer, R.G., Campbell, J., Dittmar, T., 2013. Global charcoal mobilization from soils via dissolution and riverine transport to the oceans. Science 340 (6130), 345–347.
Jin, Z., Cao, J., Wu, J., Wang, S., 2006. A Rb/Sr record of catchment weathering response to Holocene climate change in Inner Mongolia. Earth Surf. Process. Landforms: J. Br. Geomorphol. Res. Group 31 (3), 285–291.
Jin, Z., Wang, S., Shen, J.I., Zhang, E., Li, F., Ji, J., Lu, X., 2001. Chemical weathering since the Little Ice Age recorded in lake sediments: a high-resolution proxy of past climate. Earth Surf. Process. Landforms: J. Br. Geomorphol. Res. Group 26 (7), 775–782.
Juyal, N., Pant, R.K., Basavaiah, N., Bhushan, R., Jain, M., Saini, N.K., Yadava, M.G., Singhvi, A.K., 2009. Reconstruction of last glacial to early Holocene monsoon variability from relict lake sediments of the higher central Himalaya, Uttrakhand, India. J. Asian Earth Sci. 34 (3), 437–449.
Juyal, N., Pant, R.K., Basavaiah, N., Yadava, M.G., Saini, N.K., Singhvi, A.K., 2004. Climate and seismicity in the higher Central Himalaya during 20–10 ka: evidence from the Garbayang basin, Uttaranchal, India. Palaeogeogr. Palaeoclimatol. Palaeoecol. 213 (3–4), 315–330.
Juyal, N., Sundriyal, Y., Rana, N., Chaudhary, S., Singhvi, A.K., 2010. Late Quaternary fluvial aggradation and incision in the monsoon-dominated Alaknanda valley, Central Himalaya, Uttrakhand, India. J. Quat. Sci. 25 (8), 1293–1304.
Kaplan, J.O., Krumhardt, K.M., Ellis, E.C., Ruddiman, W.F., Lemmen, C., Goldewijk, K.K., 2011. Holocene carbon emissions as a result of anthropogenic land cover change. Holocene 21 (5), 775–791.
Kathayat, G., Cheng, H., Sinha, A., Yi, L., Li, X., Zhang, H., Li, H., Ning, Y., Edwards, R.L., 2017. The Indian monsoon variability and civilization changes in the Indian subcontinent. Sci. Adv. 3 (12), e1701296.
Kenoyer, J.M., 1998. Ancient Cities of the Indus Valley Civilization. American Institute of Pakistan Studies. Oxford University Press, pp. 8–96.
Kimothi, M.M., Juyal, N., 1996. Environmental impact assessment of a few selected watersheds of the Chamoli district (Central Himalaya) using remotely sensed data. Int. J. Rem. Sens. 17 (7), 1391–1405.
Knörzer, K.H., 2000. 3000 years of agriculture in a valley of the High Himalayas. Veg. Hist. Archaeobotany 9 (4), 219–222.
Kodera, K., 2004. Solar influence on the Indian Ocean Monsoon through dynamical processes. Geophys. Res. Lett. 31 (24).
Lal, B.B., 1992. The painted grey ware culture of the iron age. In: Dani, A.H., Masson, V.M. (Eds.), History of Civilizations of Central Asia 1: the Dawn of Civilization: Earliest Times to 700 B.C. UNESCO Publishing, Paris, pp. 421–440.
Leborgne, E., 1960. Influence of fire on the magnetic properties of soil, of schist, and of granite. Ann. Geograph. 16, 159–195.
Lewis, S.L., Maslin, M.A., 2015. Defining the anthropocene. Nature 519 (7542), 171–180.
Leys, B., Higuera, P.E., McLauchlan, K.K., Dunnette, P.V., 2016. Wildfires and geochemical change in a subalpine forest over the past six millennia. Environ. Res. Lett. 11 (12), 125003.
Liu, Q., Roberts, A.P., Larrasoaña, J.C., Banerjee, S.K., Guyodo, Y., Tauxe, L., Oldfield, F., 2012. Environmental magnetism: principles and applications. Rev. Geophys. 50, 1–50. RG4002.
Lowe, J.J., Walker, M., 2014. Reconstructing Quaternary Environments, third ed. Routledge Abingdon, p. 569.
Mackereth, F.J., 1966. Some chemical observations on post-glacial lake sediments. Philos. Trans. R. Soc. Lond. Ser. B Biol. Sci. 250 (765), 165–213.
Marcott, S.A., Shakun, J.D., Clark, P.U., Mix, A.C., 2013. A reconstruction of regional and global temperature for the past 11,300 years. Science 339 (6124), 1198–1201.
Mayewski, P.A., Rohling, E.E., Stager, J.C., Karlén, W., Maasch, K.A., Meeker, L.D., Meyerson, E.A., Gasse, F., van Kreveld, S., Holmgren, K., Lee-Thorp, J., 2004. Holocene climate variability. Quat. Res. 62 (3), 243–255.
McWethy, D.B., Higuera, P.E., Whitlock, C., Veblen, T.T., Bowman, D.M.J.S., Cary, G.J., Haberle, S.G., Keane, R.E., Maxwell, B.D., McGlone, M.S., Perry, G.L.W., Tepley, A.J., 2013. A conceptual framework for predicting temperate ecosystem sensitivity to human impacts on fire regimes. Global Ecol. Biogeogr. 22 (8), 900–912.
Meadow, R.H., Jansen, M.M., Urban, G., 1991. The domestication and exploitation of plants and animals in the Greater Indus Valley, 7th–2nd millennium BC. In: Jansen, M.M., Urban, G. (Eds.), Forgotten Cities on the Indus. Mainz: Philipp Von Zabern, pp. 51–58.
Moritz, M.A., Parisien, M.A., Batllori, E., Krawchuk, M.A., Van Dorn, J., Ganz, D.J., Hayhoe, K., 2012. Climate change and disruptions to global fire activity. Ecosphere 3 (6), 1–22.
Nautiyal, K.P., 1991. Emergence of Early Culture in Garhwal Central Himalaya: A Study Based on Excavations at Thapli and Ranihat. University Museum of Himalayan Archaeology and Ethnography, HN Bahuguna Garhwal University.
Nautiyal, K.P., Khanduri, B.M., 1986. New cultural dimension in the central Himalayan region of Uttarakhand an archaelogical assessment. Annali dell'Università degli Studi di Napoli “L'Orientale”. Rivista del Dipartimento di Studi Asiatici e del Dipartimento di Studi e Ricerche su Africa e Paesi Arabi (46), 77–100, 1986.
Nautiyal, V., Bhatt, R.C., Saklani, P.M., Tripathy, V.M., Nautiyal, C.M., Chauhan, H., 2014. Lippa and Kanam: Trans-Himalayan cist burial culture and pyrotechnology in Kinnaur, Himachal Pradesh, India. Antiquity 88 (5).
Nesje, A., Dahl, S.O., 1993. Lateglacial and Holocene glacier fluctuations and climate variations in western Norway: a review. Quat. Sci. Rev. 12 (4), 255–261.
O'Brien, S.R., Mayewski, P.A., Meeker, L.D., Meese, D.A., Twickler, M.S., Whitlow, S.I., 1995. Complexity of Holocene climate as reconstructed from a Greenland ice core. Science 270 (5244), 1962–1964.
Oldfield, F., Wake, R., Boyle, J., Jones, R., Nolan, S., Gibbs, Z., Appleby, P., Fisher, E., Wolff, G., 2003. The late-Holocene history of Gormire Lake (NE England) and its catchment: a multiproxy reconstruction of past human impact. Holocene 13 (5), 677–690.
PAGES Hydro2k Consortium, 2017. Comparing proxy and model estimates of hydroclimate variability and change over the Common Era. Clim. Past 13, 1851–1900.
Patterson III, W.A., Edwards, K.J., Maguire, D.J., 1987. Microscopic charcoal as a fossil indicator of fire. Quat. Sci. Rev. 6 (1), 3–23.
Popović, Z., Bojović, S., Marković, M., Cerdà, A., 2021. Tree Species Flammability Based on Plant Traits: A Synthesis, vol. 800. Science of the Total Environment, 149625.
Pyne, S.J., 2001. The fires this time, and next. Science 294 (5544), 1005–1006.
Qazi, N.Q., Bruijnzeel, L.A., Rai, S.P., Ghimire, C.P., 2017. Impact of forest degradation on streamflow regime and runoff response to rainfall in the Garhwal Himalaya, Northwest India. Hydrol. Sci. J. 62 (7), 1114–1130.
Rana, N., Sharma, S., Ali, S.N., Singh, S., Shukla, A.D., 2019. Investigating the sensitivity of glaciers to climate variability since the MIS-2 in the upper Ganga catchment (Saraswati valley), Central Himalaya. Geomorphology 346, 106854.
Randerson, J.T., Liu, H., Flanner, M.G., Chambers, S.D., Jin, Y., Hess, P.G., Pfister, G., Mack, M.C., Treseder, K.K., Welp, L.R., Chapin, F.S., Harden, J.W., Goulden, M.L., Lyons, E., Neff, J.C., Schuur, E.A.G., Zender, C.S., 2006. The impact of Boreal forest fire on climate warming. Science 314, 1130–1132.
Rasmussen, K.L., Houze, R.A., 2012. A flash-flooding storm at the steep edge of high terrain: disaster in the Himalayas. Bull. Am. Meteorol. Soc. 93 (11), 1713–1724.
Ray, Y., Srivastava, P., 2010. Widespread aggradation in the mountainous catchment of the Alaknanda–Ganga River System: timescales and implications to Hinterland–foreland relationships. Quat. Sci. Rev. 29 (17), 2238–2260.
Reimer, P.J., Austin, W.E., Bard, E., Bayliss, A., Blackwell, P.G., Ramsey, C.B., Butzin, M., Cheng, H., Edwards, R.L., Friedrich, M., Grootes, P.M., Talamo, S., 2020. The IntCal20 Northern Hemisphere radiocarbon age calibration curve (0–55 cal kBP). Radiocarbon 62 (4), 725–757.
Reimer, P.J., Bard, E., Bayliss, A., Beck, J.W., Blackwell, P.G., Ramsey, C.B., Buck, C.E., Cheng, H., Edwards, R.L., Friedrich, M., Grootes, P.M., 2013. IntCal13 and Marine13 radiocarbon age calibration curves 0–50,000 years cal BP. Radiocarbon 55 (4), 1869–1887.
Roberts, A.P., Zhao, X., Heslop, D., Abrajevitch, A., Chen, Y.H., Hu, P., Jiang, Z., Liu, Q., Pillans, B.J., 2020. Hematite (α-Fe2O3) quantification in sedimentary magnetism: limitations of existing proxies and ways forward. Geosci. Lett. 7 (1), 1–11.
Robinson, S.G., 1986. The late Pleistocene palaeoclimatic record of North Atlantic deep-sea sediments revealed by mineral-magnetic measurements. Phys. Earth Planet. In. 42 (1–2), 22–47.
Roy, I., Ranhotra, P.S., Tomar, N., Shekhar, M., Agrawal, S., Bhattacharyya, A., Kumar, P., Patil, S.K., Sharma, R., 2022. Reconstruction of the late Holocene climate variability from the summer monsoon dominant Bhagirathi valley, western Himalaya. J. Asian Earth Sci. 227, 105080.
Ruddiman, W.F., 2003. The anthropogenic greenhouse era began thousands of years ago. Climatic Change 61 (3), 261–293.
Ruddiman, W.F., Crucifix, M.C., Oldfield, F.A., 2011. The early-anthropocene hypothesis. Holocene 21 (5), 713–887.
Ruddiman, W.F., Thomson, J.S., 2001. The case for human causes of increased atmospheric $CH_4$ over the last 5000 years. Quat. Sci. Rev. 20 (18), 1769–1777.
Rupp, T.S., Chapin III, F.S., Starfield, A.M., 2000. Response of subarctic vegetation to transient climatic change on the Seward Peninsula in north west Alaska. Global Change Biol. 6 (5), 541–555.
Sarangi, V., Roy, S., Sanyal, P., 2022. Effect of burning on the distribution pattern and isotopic composition of plant biomolecules: implications for paleoecological studies. Geochem. Cosmochim. Acta 318, 305–327.
Sati, S.P., Ali, S.N., Rana, N., Bhattacharya, F., Bhushan, R., Shukla, A.D., Sundriyal, Y., Juyal, N., 2014. Timing and extent of Holocene glaciations in the monsoon dominated Dunagiri valley (Bangni glacier), Central Himalaya, India. J. Asian Earth Sci. 91, 125–136.
Scott, A.C., Damblon, F., 2010. Charcoal: taphonomy and significance in geology, botany and archaeology. Palaeogeogr. Palaeoclimatol. Palaeoecol. 291 (1), 1–10.
Scott, A.C., Glasspool, I.J., 2006. The diversification of Paleozoic fire systems and fluctuations in atmospheric oxygen concentration. Proc. Natl. Acad. Sci. 103 (29), 10861–10865.
Sharma, S., Shukla, A.D., Bartarya, S.K., Marh, B.S., Juyal, N., 2017. The Holocene floods and their affinity to climatic variability in the western Himalaya, India. Geomorphology 290, 317–334.
Shrestha, D., Singh, P., Nakamura, K., 2012. Spatiotemporal variation of rainfall over the central Himalayan region revealed by TRMM Precipitation Radar. J. Geophys. Res. Atmos. 117 (D22).
Shukla, A.D., 2011. Geochemical and Isotopic Studies of Some Sedimentary Sequences of the Vindhyan Super Group. Unpublished Ph. D. thesis submitted to MS University, India. Baroda.
Snowball, I., Thompson, R., 1990. A stable chemical remanence in Holocene sediments. J. Geophys. Res. Solid Earth 95 (B4), 4471–4479.

Solanki, S.K., Usoskin, I.G., Kromer, B., Schüssler, M., Beer, J., 2004. Unusual activity of the Sun during recent decades compared to the previous 11,000 years. Nature 431 (7012), 1084–1087.
Srivastava, P., Agnihotri, R., Sharma, D., Meena, N., Sundriyal, Y.P., Saxena, A., Bhushan, R., Sawlani, R., Banerji, U.S., Sharma, C., Bisht, P., Rana, N., Jayangondaperumal, R., 2017. 8000-year monsoonal record from Himalaya revealing reinforcement of tropical and global climate systems since mid-Holocene. Sci. Rep. 7 (1), 1–10.
Srivastava, P., Tripathi, J.K., Islam, R., Jaiswal, M.K., 2008. Fashion and phases of late Pleistocene aggradation and incision in the Alaknanda River valley, western Himalaya, India. Quat. Res. 70 (1), 68–80.
Stephens, L., Fuller, D., Boivin, N., Rick, T., Gauthier, N., Kay, A., Marwick, B., Armstrong, C.G., Barton, C.M., Denham, T., Douglass, K., 2019. Archaeological assessment reveals Earth's early transformation through land use. Science 365 (6456), 897–902.
Sundriyal, Y.P., Tripathi, J.K., Sati, S.P., Rawat, G.S., Srivastava, P., 2007. Landslide-dammed lakes in the Alaknanda basin, lesser Himalaya: causes and implications. Curr. Sci. 93 (4), 568–574.
Sundriyal, Y.P., Shukla, A.D., Rana, N., Jayangondaperumal, R., Srivastava, P., Chamyal, L.S., Sati, S.P., Juyal, N., 2015. Terrain response to the extreme rainfall event of June 2013: evidence from the Alaknanda and Mandakini river valleys, Garhwal Himalaya, India. Episodes 38 (3), 179–188.
Swetnam, T.W., 1993. Fire history and climate change in giant sequoia groves. Science 262 (5135), 885–889.
Tewari, R., 2003. The origins of iron working in India: new evidence from the Central Ganga Plain and the Eastern Vindhyas. Antiquity 77 (297), 536–544.
Turner, G.M., 1997. Environmental magnetism and magnetic correlation of high resolution lake sediment records from Northern Hawke's Bay, New Zealand. N. Z. J. Geol. Geophys. 40 (3), 287–298.
Vance, D., Bickle, M., Ivy-Ochs, S., Kubik, P.W., 2003. Erosion and exhumation in the Himalaya from cosmogenic isotope inventories of river sediments. Earth Planet Sci. Lett. 206 (3), 273–288.
Vandenberghe, J., 2015. River terraces as a response to climatic forcing: formation processes, sedimentary characteristics and sites for human occupation. Quat. Int. 370, 3–11.
Vannière, B., Power, M.J., Roberts, N., Tinner, W., Carrión, J., Magny, M., Bartlein, P., Colombaroli, D., Daniau, A.L., Finsinger, W., Gil-Romera, G., Vescovi, E., 2011. Circum-Mediterranean fire activity and climate changes during the mid-Holocene environmental transition (8500-2500 cal. BP). Holocene 21 (1), 53–73.
Vellore, R.K., Kaplan, M.L., Krishnan, R., Lewis, J.M., Sabade, S., Deshpande, N., Singh, B.B., Madhura, R.K., Rama Rao, M.V.S., 2016. Monsoon-extratropical circulation interactions in Himalayan extreme rainfall. Clim. Dynam. 46 (11), 3517–3546.
Verosub, K.L., Roberts, A.P., 1995. Environmental magnetism: past, present, and future. J. Geophys. Res. Solid Earth 100 (B2), 2175–2192.
Wang, H., Liu, H., Cui, H., Abrahamsen, N., 2001. Terminal Pleistocene/Holocene palaeoenvironmental changes revealed by mineral-magnetism measurements of lake sediments for Dali Nor area, southeastern Inner Mongolia Plateau, China. Palaeogeogr. Palaeoclimatol. Palaeoecol. 170 (1), 115–132.
Wasson, R.J., Sundriyal, Y.P., Chaudhary, S., Jaiswal, M.K., Morthekai, P., Sati, S.P., Juyal, N., 2013. A 1000-year history of large floods in the Upper Ganga catchment, central Himalaya, India. Quat. Sci. Rev. 77, 156–166.
Wasson, R.J., Juyal, N., Jaiswal, M., McCulloch, M., Sarin, M.M., Jain, V., Srivastava, P., Singhvi, A.K., 2008. The mountain-lowland debate: deforestation and sediment transport in the upper Ganga catchment. J. Environ. Manag. 88 (1), 53–61.
Weir, J.R., Limb, R.F., 2013. Seasonal variation in flammability characteristics of Quercus marilandica and Quercus stellata leaf litter burned in the laboratory. Fire Ecol. 9 (3), 80–88.
Whitlock, C., Higuera, P.E., McWethy, D.B., Briles, C.E., 2010. Paleoecological perspectives on fire ecology: revisiting the fire-regime concept. Open Ecol. J. 3 (1).
Whitlock, C., Larsen, C., 2002. Charcoal as a fire proxy. In: Tracking Environmental Change Using Lake Sediments. Springer, Dordrecht, pp. 75–97.
Wright, R.P., Bryson, R.A., Schuldenrein, J., 2008. Water supply and history: Harappa and the Beas regional survey. Antiquity 82 (315), 37–48.
Wright, R.P., 2010. The Ancient Indus: Urbanism, Economy, and Society. Cambridge University Press, Cambridge, p. 396.
Wu, D., Zhou, A., Liu, J., Chen, X., Wei, H., Sun, H., Yu, J., Bloemendal, J., Chen, F., 2015. Changing intensity of human activity over the last 2,000 years recorded by the magnetic characteristics of sediments from Xingyun Lake, Yunnan, China. J. Paleolimnol. 53 (1), 47–60.
Zhisheng, An, et al., 2011. Glacial-Interglacial Indian Summer Monsoon Dynamics. Science 333, 719–723.